



# Parallel Nonfunctionalization of CK1 $\delta/\epsilon$ Kinase Ohnologs Following a Whole-Genome Duplication Event

Daniel Evans-Yamamoto <sup>1,2,3,4,5,6,7</sup>, Alexandre K. Dubé,<sup>1,2,3,4,5,†</sup> Gourav Saha,<sup>1,2,3,4,5,8,9,†</sup> Samuel Plante,<sup>1,2,3,4,5,10</sup> David Bradley,<sup>1,2,3,4,5</sup> Isabelle Gagnon-Arsenault,<sup>1,2,3,4,5</sup> and Christian R. Landry <sup>1,2,3,4,5,6,\*</sup>

<sup>1</sup>Institut de Biologie Intégrative et des Systèmes (IBIS), Université Laval, Québec, QC, G1V 0A6, Canada

<sup>2</sup>Département de Biochimie, de Microbiologie et de Bio-informatique, Faculté des Sciences et de Génie, Université Laval, Québec, QC, G1V 0A6, Canada

<sup>3</sup>Département de Biologie, Faculté des Sciences et de Génie, Université Laval, Québec, QC, G1V 0A6, Canada

<sup>4</sup>PROTEO, Le regroupement québécois de recherche sur la fonction, l'ingénierie et les applications des protéines, Université Laval, Québec, QC, G1V 0A6, Canada

<sup>5</sup>Centre de Recherche sur les Données Massives (CRDM), Université Laval, Québec, QC, G1V 0A6, Canada

<sup>6</sup>Systems Biology Program, Graduate School of Media and Governance, Keio University, Fujisawa, Kanagawa, 252-0882, Japan

<sup>7</sup>Institute for Advanced Biosciences, Keio University, Fujisawa, Kanagawa, 252-0882, Japan

<sup>8</sup>Department of Biological Sciences, Birla Institute of Technology and Science, Pilani K K Birla Goa Campus, South Goa, India

<sup>9</sup>Present address: Department of Bioengineering, University of California, Los Angeles, CA, 90095, USA

<sup>10</sup>Present address: Département de Biochimie, Université de Sherbrooke, Québec, QC, J1K 0A5, Canada

<sup>†</sup>These authors contributed equally to this work.

\*Corresponding author: E-mail: christian.landry@bio.ulaval.ca.

Associate editor: Naruya Saitou

## Abstract

Whole-genome duplication (WGD) followed by speciation allows us to examine the parallel evolution of ohnolog pairs. In the yeast family *Saccharomycetaceae*, *HRR25* is a rare case of repeated ohnolog maintenance. This gene has reverted to a single copy in *Saccharomyces cerevisiae* where it is now essential, but has been maintained as pairs in at least 7 species post-WGD. In *S. cerevisiae*, *HRR25* encodes the casein kinase 1 $\delta/\epsilon$  and plays a role in a variety of functions through its kinase activity and protein–protein interactions (PPIs). We hypothesized that the maintenance of duplicated *HRR25* ohnologs could be a result of repeated subfunctionalization. We tested this hypothesis through a functional complementation assay in *S. cerevisiae*, testing all pairwise combinations of 25 orthologs (including 7 ohnolog pairs). Contrary to our expectations, we observed no cases of pair-dependent complementation, which would have supported the subfunctionalization hypothesis. Instead, most post-WGD species have one ohnolog that failed to complement, suggesting their nonfunctionalization or neofunctionalization. The ohnologs incapable of complementation have undergone more rapid protein evolution, lost most PPIs that were observed for their functional counterparts and singletons from post-WGD and non-WGD species, and have nonconserved cellular localization, consistent with their ongoing loss of function. The analysis in *Naumovozyma castellii* shows that the noncomplementing ohnolog is expressed at a lower level and has become nonessential. Taken together, our results indicate that *HRR25* orthologs are undergoing gradual nonfunctionalization.

**Key words:** whole-genome duplication, gene retention, ohnologs, nonfunctionalization, protein kinase, protein–protein interactions.

## Introduction

One of the driving forces behind the evolution of complex traits and the diversification of species is gene duplication (Otto and Whitton 2019; Donoghue and Purnell 2005). Although most genes are duplicated at one point or another during their evolutionary history, only a fraction will be retained in some lineages as duplicated pairs or

as part of larger families. Identifying the molecular mechanisms and population dynamics parameters that dictate the retention of some gene duplicates, but not others, is a major goal in molecular evolution.

The classical model for the maintenance of gene duplication posits that due to its redundancy, a duplicated gene is now free to explore a new sequence space and therefore can gain new, adaptive functions that favor its

**Received:** September 26, 2023. **Accepted:** November 07, 2023

© The Author(s) 2023. Published by Oxford University Press on behalf of Society for Molecular Biology and Evolution.

This is an Open Access article distributed under the terms of the Creative Commons Attribution-NonCommercial License (<https://creativecommons.org/licenses/by-nc/4.0/>), which permits non-commercial re-use, distribution, and reproduction in any medium, provided the original work is properly cited. For commercial re-use, please contact [journals.permissions@oup.com](mailto:journals.permissions@oup.com)

**Open Access**

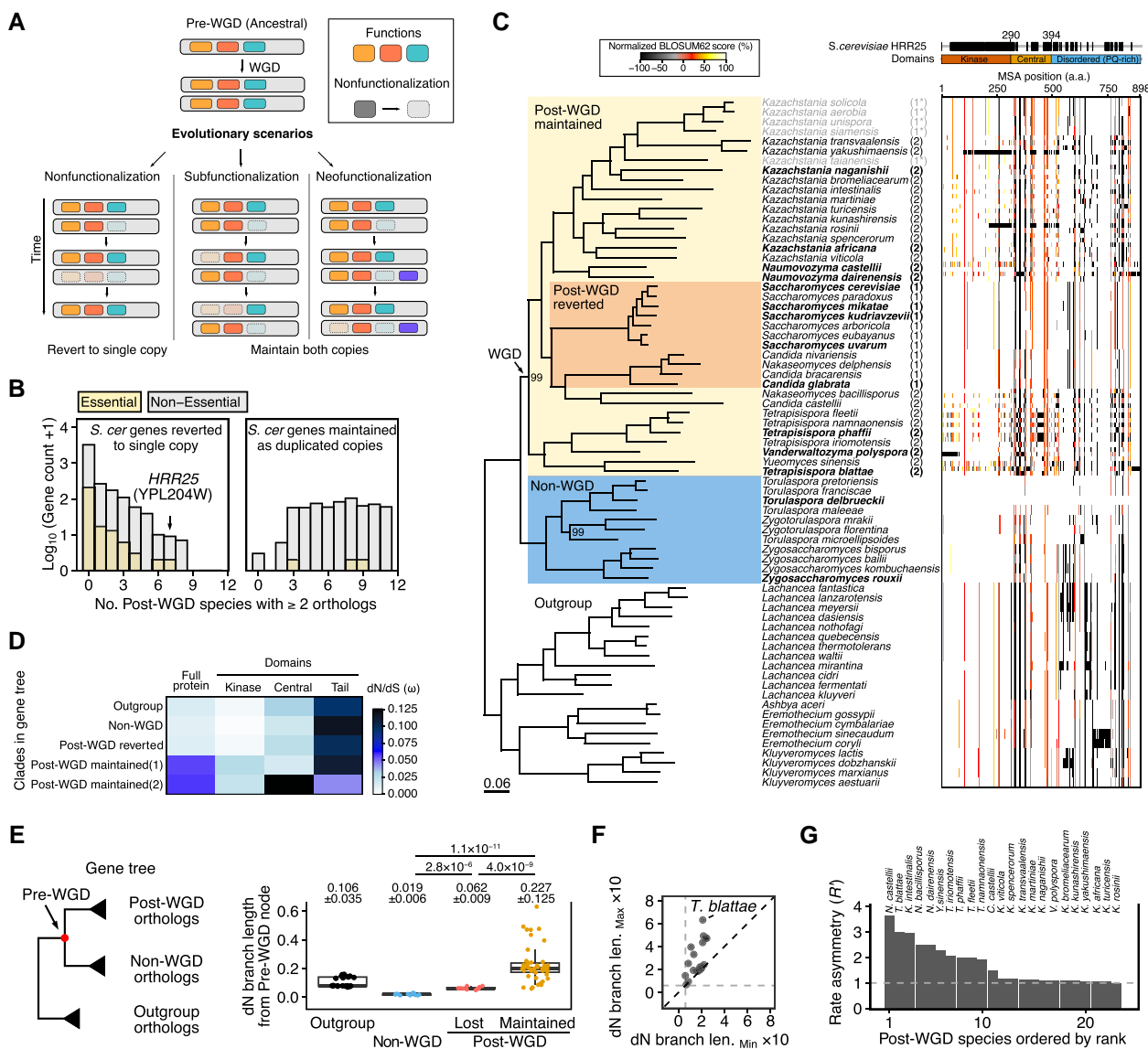


**Fig. 1.** Conservation and divergence of *HRR25* ohnologs in the *Saccharomycetaceae* family after Whole-Genome Duplication (WGD). **A**) Diagram of evolutionary fates of ohnologs after WGD. (Left) One of the ohnologs accumulates mutations and nonfunctionalizes. (Middle) Subfunctionalization: Two copies are partially degenerating, each preserving parts of the ancestral functions. (Right) Neofunctionalization: one copy maintains the ancestral function and another gains novel functions. **B**) Number of post-WGD species that maintained both ohnologs for essential and nonessential *S. cerevisiae* genes and separated by status in *S. cerevisiae*. *HRR25* is an exceptional case of ohnologs that were maintained in several species while returning to a single copy in *S. cerevisiae*. **C**) (Left) Phylogenetic tree of *Saccharomycetaceae*, adapted from Li et al. (2021). Confidence annotations for branches with bootstrap confidence of 100 are abbreviated. Post-WGD species are annotated with respect to the numbers of *HRR25* copies. Species used for homology search are shown in bold. Species with low confidence for copy number annotation are in light gray and number is marked with an asterisk. (Right) Multiple sequence alignment (MSA) of *Hrr25p*. Normalized BLOSUM62 score for divergence with the non-WGD *T. delbrueckii* ortholog (TDEL0E05230). The aligned region of *S. cerevisiae* *Hrr25p* is indicated on top as black boxes, together with domain annotation. **D**) The ratio of nonsynonymous to synonymous substitutions ( $dN/dS$  value,  $\omega$ ) of *HRR25*, by clade and domain. Domains are as in C). Gene tree is shown in [supplementary fig. S1, Supplementary Material](#) online. **E**) Evolutionary distance among *Hrr25p* orthologs. (Left) Schematic of the gene tree. Branch lengths from the Pre-WGD node (shown in red) were computed using the tree based on nonsynonymous changes ( $dN$ ), with the tree structure shown in [supplementary fig. S1, Supplementary Material](#) online. (Right) Branch lengths from the pre-WGD node, by maintenance status of *HRR25*. Mean  $\pm$  SD is shown for each group. The difference in group means is compared with a two-sided Wilcoxon test. **F**) Scatter plot representation of  $dN$  tree branch lengths for post-WGD species maintaining two ohnologs of *HRR25*. Gray dashed line represents the mean of post-WGD orthologs which reverted to single copy state. Black dashed line shows  $x = y$ . **G**) Asymmetrical evolution of ohnologs by species. Rate asymmetry ( $R'$ ) for each post-WGD species maintaining two copies of *HRR25*.  $R'$  values were computed as the ratio of values represented in D) by dividing the value of the ohnolog with longer branch length with the ohnolog with the shorter branch length as in Byrne and Wolfe (2007). Gray dashed line represents  $R' = 1$ , where evolutionary rates of both ohnologs are equivalent.

maintenance (Ohno 1970; Fig. 1A). Another alternative model is that since genes have multiple functions and loss of function through mutations is generally more likely

than gain of function, duplicated genes could simply partition the ancestral function and functionally complement each other, resulting in two genes that together only can

perform the ancestral function (subfunctionalization) (Hughes 1994; Force et al. 1999). In this model, the paralogs degenerate and eventually complement each other (DDC; Duplication, Degeneration and Complementation). These models apply not only to protein functions but also to their expression. For instance, gene duplication could simply increase protein dosage and that in itself could be adaptive, leading to the maintenance of the 2 genes with no necessary changes in the intrinsic molecular functions of the proteins (Innan and Kondrashov 2010; Kondrashov 2010). Indeed, increases in gene copy number have been shown to be adaptive in many cases (Perry et al. 2007; Pajic et al. 2019; Ascencio et al. 2021). When increased expression is not adaptive, subfunctionalization could occur at the level of expression alone. For instance, if duplicates evolve to have lower expression levels after gene duplication, the paralogs as a pair are required to achieve the dosage that is needed to perform the ancestral function (Qian et al. 2015; Gout and Lynch 2015). In this case again, no divergence of function is required. However, once divergence in expression becomes asymmetrical, the asymmetry could enhance with time and the least expressed paralog could get to a level of expression low enough that further degenerative mutations affecting expression, function, or stability would become effectively neutral. Therefore, although initially the genes are maintained by dosage subfunctionalization, this mechanism could eventually promote slow gene loss in the long term (Gout and Lynch 2015). Gene loss through nonfunctionalization eventually occurs via this model but not as rapidly as it would have if loss-of-function mutations occurred soon after gene duplication.

Although it is challenging to determine the exact mechanisms that led to the retention of a specific gene pair, each of these models make specific predictions regarding duplication, most of which have been tested in the budding yeast. The ancestor of some clades of the yeast family *Saccharomycetaceae* underwent a whole-genome duplication (WGD) that has impacted their cellular network architecture and functions. About 15% of ohnologs were maintained as pairs in the lineage leading to *Saccharomyces cerevisiae*, while the other 85% have returned to single copy (Byrne and Wolfe 2005). The systematic study of the remaining ohnolog pairs revealed patterns of retention that are consistent with the various models outlined above. We will not review this rich literature here, but we will illustrate with a few cases.

A classical paper (van Hoof 2005) for instance tested the DDC model using complementation tests. In this model, duplicates are maintained by partitioning the ancestral function. The author showed that for at least three pairs of genes, the diverged functions of ohnologs could be complemented with an orthologous gene from a species that diverged prior to the WGD. One of the reasons why WGDs are powerful model systems for the study of gene duplication is that speciation events that occur after the WGD event lead to opportunities for repeated, partially independent gene pair maintenance in these species. For instance, the

comparison of *S. cerevisiae* and *Kluyveromyces polysporus* (also known as *Vanderwaltozyma polyspora*; Scannell et al. 2007) showed that genes associated with particular molecular functions were more or less likely to be retained after the WGD. One specific example was that both species showed an underrepresentation of RNA metabolism genes among the preserved ohnologs, but an over representation of protein kinases. In other studies, it was shown that data on the evolution of gene expression in various species support the model of dosage subfunctionalization, where duplicated genes show decreased expression levels, partitioning the dosage requirements between the two copies (Qian et al. 2015; Gout and Lynch 2015). The Gout and Lynch model shows that maintaining constant summed expression could result in neutral evolution, which gradually creates an imbalance of expression between ohnologs, leading to the nonfunctionalization of one copy.

Here, we examined ohnologs that were maintained across many species, not focusing on their maintenance in *S. cerevisiae* alone. We searched for cases so that we could compare, for a given gene, multiple pairs of ohnologs that may be undergoing different fates in different species. We found one particular case, *HRR25*, that we examined in detail, and combined multiple approaches to dissect their potential fate. The casein kinase 1 $\delta/\epsilon$  (gene *HRR25* in *S. cerevisiae*) is present in many eukaryotic proteomes where it phosphorylates serine or threonine residues on its numerous substrates (Tanaka et al. 2014). This kinase plays a role in a variety of functions, including endocytosis (Peng et al. 2015a), DNA damage repair (Hoekstra et al. 1991), ribosome biogenesis (Ghalei et al. 2015), meiosis (Ye et al. 2016; Zhang et al. 2018), autophagy (Pfaffenwimmer et al. 2014), and membrane trafficking (Wang et al. 2015). The deletion of this gene causes inviability in the laboratory strain of *S. cerevisiae* (Giaever et al. 2002), and mutations in the P-body localization signal (PLS) sequence or heterozygous deletion of the entire gene result in the failure of spore formation (Zhang et al. 2018).

The maintenance of both *HRR25* duplicate copies and its large number of functions make it a good model to examine its pattern of molecular evolution following the yeast WGD. We examined whether the ohnologs have most likely been maintained by subfunctionalization or neofunctionalization, or if they may be slowly undergoing nonfunctionalization. To test the predictions of these various models, we examined the rate of evolution of the ohnologs and we performed functional complementation assays in *S. cerevisiae*, using the essentiality of the *S. cerevisiae* singleton as a phenotype. We did so by measuring the effects of their expression on cell viability while conditionally repressing the endogenous *HRR25*. We investigated the molecular mechanisms for the observed viability by performing proteome-wide protein–protein interaction (PPI) assays. The orthologs with similar PPI profiles to *S. cerevisiae* Hrr25p matched with that of the orthologs capable of complementation. Most of the ohnolog pairs exhibited one ohnolog that cannot complement and also drastically lost its PPIs, suggesting nonfunctionalization. Localization

analysis also showed that the orthologs incapable of functional complementation have distinct patterns of subcellular localization, similar to that of a catalytic dead mutant reported in previous studies. We validated this finding in *Naumovozyma castellii*, showing that one ohnolog of this species has become nonessential. Taken together, we show that ohnologs of *HRR25*, a kinase under strong negative selection when present in singleton, are undergoing asymmetrical evolution and have functional features that are consistent with their nonfunctionalization.

## Results and Discussion

### *HRR25* Maintenance in Post-WGD *Saccharomycetaceae* Species are Asymmetrical in Evolutionary Rates

Previous efforts have annotated the genomes of non-WGD and post-WGD species, and identified cases of gene maintenance and losses (Byrne and Wolfe 2005). Using this resource, we performed a preliminary analysis to search for cases of essential genes in *S. cerevisiae*, which reverted to the single copy state in this model species, but having both duplicated copies maintained in other post-WGD species. We found that *HRR25*, a gene coding for the kinase CK1 $\delta/\epsilon$ , is a rare case where both duplicated copies are maintained in 7 species post-WGD, which is much more than for other *S. cerevisiae* genes (mean = 0.31, Z-score = 7.3, Fig. 1B). Multiple sequence alignment of orthologs and the comparison with the ortholog of non-WGD species *Torulaspora delbrueckii* showed that species which maintained both *HRR25* ohnologs have lower sequence identity compared with non-WGD or single reverted state species (Fig. 1C). This suggests that in species where both ohnologs are maintained, this kinase has been evolving faster.

We therefore examined the molecular evolution of orthologs by constructing a gene tree from protein sequences (supplementary fig. S1, Supplementary Material online). The ratio of nonsynonymous to synonymous substitutions ( $dN/dS$  value,  $\omega$ ) was used to estimate the strength of selection acting on these genes. The  $\omega$  value for *HRR25*, based on a homogeneous model, is 0.035, suggesting that it is under strong negative/purifying selection. We then asked if gene duplication relaxed the degree of purifying selection on *HRR25* orthologs. We examined this using a branch model to estimate an overall  $\omega$  in post-WGD orthologs. We found that  $\omega$  increased for two clades which contain orthologs from post-WGD species maintaining both ohnologs ( $\omega = 0.058$  and  $0.056$ ), compared with clades with post-WGD species that reverted to single copy ( $\omega = 0.013$ ), non-WGD species ( $\omega = 0.011$ ), and the outgroup ( $\omega = 0.014$ ) (supplementary fig. S1, Supplementary Material online). This shows that purifying selection has been relaxed specifically for orthologs in species that maintained both ohnologs.

In *S. cerevisiae*, *Hrr25p* has three domains: the kinase domain, the central domain, and the tail region (Corbett and Harrison 2012). The disordered C-terminal tail region has a

high proline and glutamine content, and undergoes autophosphorylation to form a pseudosubstrate inhibitor that affects the activity and specificity of the kinase (Cullati et al. 2023). The central domain, packed tightly against the kinase C-lobe, is known to interact with other proteins, which is critical for the proper localization of the kinase (Ye et al. 2016). We asked whether selection differs among the three domains. Relaxation of selection occurred most strongly on the disordered tail region, followed by the central and kinase domains (Fig. 1D). In spite of its overall higher conservation level, both of the two post-WGD clades of species that maintained ohnologs show an increase of  $\omega$  value in the kinase domain. On the contrary, one post-WGD clade (annotated as post-WGD maintained 2 in Fig. 1; supplementary fig. S1, Supplementary Material online) showed larger and smaller  $\omega$  values for the central and tail domains, respectively, compared with other clades.

The difference in evolutionary rates among post-WGD ohnologs was further assessed using branch lengths from the pre-WGD node to all extant orthologs in the gene tree, which was constructed from nonsynonymous substitutions (hereafter referred to as  $dN$  tree). The mean of branch lengths for orthologs from species that maintained both ohnologs post-WGD showed significantly larger values compared with non-WGD and single copy reverted post-WGD orthologs (mean  $\pm$  SD; non-WGD:  $0.019 \pm 0.006$ ; post-WGD single copy:  $0.062 \pm 0.009$ ; post-WGD duplicate maintained:  $0.227 \pm 0.125$ ,  $P$ -value  $\leq 4.00 \times 10^{-9}$ , 2-sided Wilcoxon test) (Fig. 1E). Our observation is consistent with a previous report showing that genes on average undergo rapid evolution post-WGD, followed by subsequent decline in rate of evolution (Scannell and Wolfe 2008). The branch lengths for ohnolog pairs for species maintaining both duplicates post-WGD show that  $dN$  is variable between species and also between ohnologs maintained in the same species (Fig. 1F). To further examine the asymmetry, we measured rate asymmetry ( $R'$ ) for each pair of ohnologs by taking the ratio of their branch lengths from the  $dN$  tree (Byrne and Wolfe 2007). The rate asymmetry ( $R'$ ) of *HRR25* ohnologs pairs is highly variable among species, with *N. castellii* having the most asymmetrical rate of evolution among all pairs (Fig. 1G). To make sure that the high rate of evolution did not result from a sequencing error in the reference genome, we verified the coding sequence of *HRR25* in the *N. castellii* type strain using Sanger sequencing, and found that the sequence was correct.

### Combinatorial Complementation Assay Reveals no Subfunctionalization of *HRR25* Post-WGD

The analyses of protein sequences show that the rate of evolution for *HRR25* post-WGD has globally increased in species in which both ohnologs are maintained, and in many cases are asymmetrical between ohnologs. This increase in rate of evolution is most likely not a consequence of adaptive evolution, but of relaxed purifying selection, with a 5-fold increase in  $dN/dS$  but that remained below



1 (supplementary fig. S1, Supplementary Material online). This degree of relaxed selection, not reaching neutral evolution, is a trend also seen genome-wide for genes under negative selection post-WGD (Kondrashov et al. 2002).

We used a functional complementation assay to test if preserved ohnologs could perform the essential functions the gene has in *S. cerevisiae*. Each ortholog was expressed in *S. cerevisiae* to test if it can rescue the growth defect caused by the conditional repression of the *HRR25* (Fig. 2A and B). We synthesized all yeast orthologs ( $n = 20$ , except *S. cerevisiae*) and cloned them in a CEN plasmid (low-copy number) using the same promoter for all genes so we could control for expression. For completeness, we also included four orthologs from *Homo sapiens* as reports have shown that the human ortholog CSNK1E (but not CSNK1D nor CSNK1A1) can complement the *S. cerevisiae* *HRR25* (Laurent et al. 2020). We confirmed that all orthologs were expressed in *S. cerevisiae* using Western blotting (supplementary fig. S2, Supplementary Material online).

If the orthologs underwent subfunctionalization of essential functions, growth rescue will be achieved only when expressing both orthologs within pairs since they are expected to have complementary functions. Furthermore, if subfunctionalization took place for the same functions in different post-WGD species, orthologs from two species could also have complementary functions and be capable of complementing the function of *HRR25* as a pair. For cases where ohnolog pairs have undergone asymmetrical evolution through relaxed selection (e.g. *N. castellii*, *Tetrapispora blattae*, etc.), we expect the copy which evolved faster to fail to complement, if rapid evolution is leading to nonfunctionalization. Cases where both ohnologs are evolving at similar rates (*Kazachstania africana*, *Kazachstania naganishii*, and *V. polyspora*) are all expected to show functional complementation, since they are more likely to have maintained the ancestral functions. If orthologs have undergone neofunctionalization, only one of the ohnologs, which kept the ancestral function, will achieve complementation if functions were lost in the ohnolog that gained a new function. If the gain of functions were not accompanied with loss of other functions, both ohnologs should complement. In order to test all of these predictions, functional complementation was assayed in a combinatorial manner, testing two orthologs encoded on separate plasmids in the same cell. In order to easily associate genes to their ability to functionally complement, genes were annotated with the encoded loci (e.g. A and B) from the YGOB database (Byrne and Wolfe 2005) in upper or lower cases, to describe functional complementation and failure of complementation, respectively.

We found that all single copy orthologs, including orthologs from the species that did not undergo WGD (*Zygosaccharomyces rouxii* and *T. delbrueckii*), fully complement the repression of *HRR25* in *S. cerevisiae*, just as the *S. cerevisiae* gene does. This confirms that the function that is now essential in *S. cerevisiae* was present in the common ancestor of the post-WGD species. We observed no pair-dependent growth complementation, which was

expected in the case of subfunctionalization where ohnologs within pairs would have complementary functions (Fig. 2C). Instead, for species that maintained both ohnologs, at least one could, but most often not both, complement the repression of the *S. cerevisiae* *HRR25*. The orthologs which failed to complement were from *N. castellii*, *Naumovozyma dairenensis*, *V. polyspora*, *Tetrapispora phaffii*, and *T. blattae*. Such orthologs, except for *V. polyspora*, have all evolved faster than their counterpart ohnolog, and are likely evolving under relaxed selection. Species for which ohnologs were evolving at similar rates (*K. africana*, *K. naganishii*, and *V. polyspora*) showed complementation for both orthologs, except for *V. polyspora*. The noncomplementing *V. polyspora* ohnolog, Kpol1033p51 (b), has a frameshift mutation likely causing the mRNA to translate from an alternative start codon, resulting in a partial kinase domain.

We did not observe any complementation from any of the human orthologs. The failure of complementation for CSNK1E, which was previously reported to complement (Laurent et al. 2020), can be attributed to the difference in experimental settings such as the promoter and the exact isoforms used for the assay. We therefore focused only on the yeast orthologs for the downstream analysis. Globally, we observed a negative correlation between evolutionary rate and complementation score (see the Materials and Methods section), confirming further the association between the rate of evolution and the preservation of the ancestral functions (Fig. 2D; Pearson correlation coefficient,  $\rho = -0.786$ ,  $P\text{-value} = 4.00 \times 10^{-5}$ ).

We asked if the failure of complementation can be attributed to the loss of catalytic activity of the kinase domain, since it is the protein domain with an enzymatic activity. We investigated critical residues whose mutations cause the kinase to become pseudokinases (Kung and Jura 2019). In *HRR25*, these residues correspond to the  $\beta 3$  lysine (K38) within the VAIK motif, the aspartate (D128) in the HRD motif, and the aspartate (D149) in the DFG motif. Additionally, in *HRR25*, the mutant T176I has been reported to create a kinase dead mutant (Murakami et al. 1999). A previous study in the mammalian homolog CK1δ (CSNK1D) has reported that similar mutations (K38M and T176I) alter the localization of the protein (Milne et al. 2001) (Fig. 2E). The post-WGD orthologs did not show mutations in these motifs, but rather showed accumulation of mutations in the activation loop and substrate-binding regions, including positions that are conserved among *S. cerevisiae* kinases (YCK1, YCK2, YCK3, and *HRR25*) (Fig. 2F). We therefore hypothesized that the evolution of the kinase domain could be sufficient to cause the inability of functional complementation. We focused on *S. cerevisiae* and *N. castellii* orthologs, since *N. castellii* ohnologs have shown the most asymmetrical evolution among post-WGD species. We constructed chimeric *HRR25* genes by swapping the kinase domain between *S. cerevisiae* and *N. castellii* genes. Complementation assay of chimeric subunits showed no complementation for all constructs containing the kinase domain of the noncomplementing *N. castellii*

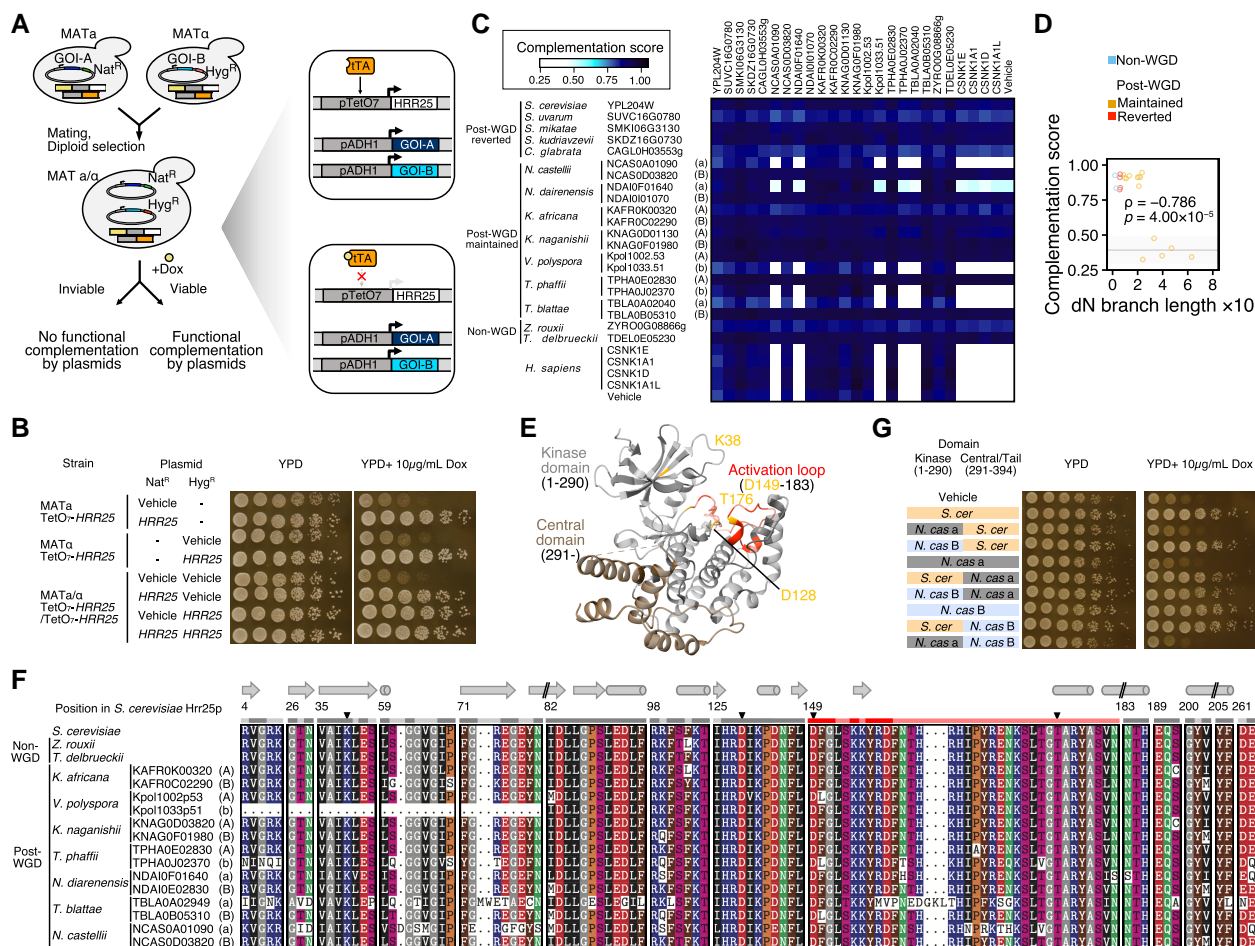


**Fig. 2.** Most ohnolog pairs have one complementing and one noncomplementing gene, and the kinase domain is critical for this complementation. A) The expression of the genomic *HRR25* in *S. cerevisiae* was put under the control of the TetO<sub>7</sub> promoter. Gene expression under the TetO<sub>7</sub> promoter requires tTA, which is inhibited in the presence of DOX. Genes expressed on the CEN/ARS plasmids under the *ADH1* promoter are not affected by the presence of DOX. Functional complementation is assessed based on the rescue of the inviable phenotype caused by repression of the endogenous *HRR25* with orthologs expressed on the CEN/ARS plasmid. GOI, gene of interest. B) Functional complementation shown by spot dilution assays. Growth of diploid strains carrying CEN/ARS plasmids that constitutively express *HRR25* under the *ADH1* promoter. Spot assay with vehicle (plasmid backbone) and with the WT *HRR25* are shown as reference. In the absence of plasmid containing the WT *HRR25*, growth is severely diminished. Expressing *HRR25* from two plasmids does not diminish growth in a detectable manner. Spots were plated in 5-fold serial dilutions, starting from OD<sub>600 nm</sub> = 0.5. C) Heatmap representation of complementation scores for combinations of orthologs. Complementation scores are relative growth, measured by growth curves of colonies on plates, under DOX divided by the YPD control ( $n = 22$  replicated colonies per genotype). Ohnologs are annotated either with A or B, corresponding to the genomic loci, based on the YGOB database. Noncomplementing ohnologs are labeled with lower case (a or b). Vehicle: Plasmid backbone with no ortholog. D) Scatter plot of complementation scores and rates of evolution. Rates of evolution are *dN* values from the tree from the pre-WGD node (shown in Fig. 1E). The gray line and shaded area indicate mean and 95% confidence interval for the vehicle control, respectively. Value for *S. cerevisiae* was excluded from this analysis. Pearson correlation ( $\rho = -0.786$ ,  $P$ -value =  $4.00 \times 10^{-5}$ ). E) Crystal structure of the *S. cerevisiae* Hrr25p [PDB: 5CYZ (Ye et al. 2016)]. The kinase domain is colored gray. Known critical residues for catalytic activity are colored orange. The activation loop within the kinase domain is colored red. The central domain is colored brown. Darker shades within the kinase domain represent positions that are conserved in the *S. cerevisiae* kinases *HRR25*, *YCK1*, *YCK2*, and *YCK3* (Murakami et al. 1999). F) Multiple sequence alignments of ohnologs showing the conserved residues in the kinase domain. Post-WGD species are ordered based on evolutionary asymmetry (*R*) values. Protein positions for *S. cerevisiae* are shown on top. Positions which correspond to helix or sheet structures are annotated above. Critical residues for catalytic activity are annotated with black triangles. Conservation of residues within *S. cerevisiae* is shown under the protein positions, with the color code as in E). G) Spot dilution assay to test for the complementation of chimeric genes to assess the role of the kinase domain in complementing the *S. cerevisiae* *HRR25*. The kinase domain (positions corresponding to 1 to 290 in *S. cerevisiae* *HRR25*) were swapped between *S. cerevisiae* and *N. castellii* orthologs. *S. cer*: *S. cerevisiae* *HRR25*; *N. cas* (a): *N. castellii* NCAS0A01090 (a); *N. cas* (b): *N. castellii* NCAS0D03820 (B). Cells were spotted in 5-fold dilution series, starting at OD<sub>600 nm</sub> = 0.5.

NCAS0A01090 (a), while the central and tail domains did not alter the functional complementation of *S. cerevisiae* or the functional *N. castellii* NCAS0D03820 (B) (Fig. 2F). This illustrates that the difference in complementation

capability of the *N. castellii* ohnologs are a result of differences in kinase domain activity.

Taken together, we observed results that are overall consistent with the nonfunctionalization of many *HRR25*

ohnologs, but not subfunctionalization nor neofunctionalization at the gene level.

### Proteome-Wide PPI Profiles Reveal Some Gains but Mostly Loss of PPIs

We wanted to further examine the functionality of HRR25 ohnologs. For this, we mapped PPIs because the pattern of PPIs with partners is a powerful indicator for the function of proteins (Marcotte et al. 1999; Mayer and Hieter 2000; Hishigaki et al. 2001).

We performed a proteome-wide DHFR-PCA screening using Hrr25p orthologs as bait and *S. cerevisiae* proteins as preys. We focused on all *S. cerevisiae* proteins that have been shown to have at least one PPI with this experimental approach (Tarassov et al. 2008; Rochette et al. 2015; Diss et al. 2017). Among the 1,172 *S. cerevisiae* proteins subjected to screening, 1,085 proteins passed the quality check for interaction evaluation (see the Materials and Methods section for details). We identified 115 proteins that interacted with at least one Hrr25p ortholog (Fig. 3A). We performed gene ontology (GO) enrichment analysis on the detected interaction partners. Significant enrichment was observed for GO terms with descriptions of cytoskeleton, cellular bud, endocytotic patch, vesicle, and cytoplasmic ribonucleoprotein granule (P-bodies) (Fig. 3B; supplementary table S7, Supplementary Material online), which agrees with previous reports for Hrr25p function (Wang et al. 2015; Peng et al. 2015a, b; Zhang et al. 2016).

We observed major differences in GO enrichment within ohnolog pairs, due to loss of individual PPIs for the non-complementing and rapidly evolving ohnologs, namely for *N. castellii* NCAS0A01090 (a), *V. polyspora* Kpol1033p51 (b), *T. blattae* TBLA0A02040 (a), *N. dairenensis* NDAI0F01640 (a), and *T. phaffii* TPHA0J02370 (b). This contrasts with the matching complementing ohnologs, which showed similar GO enrichment profiles as the non-WGD and single copy post-WGD orthologs. The similarity of PPI profiles compared with the *S. cerevisiae* Hrr25p showed a positive correlation with the functional complementation (Pearson correlation coefficient,  $\rho = 0.551$ ,  $P\text{-value} = 5.30 \times 10^{-3}$ ), which indicates that the PPI differences, mainly the losses, mirror the ability to complement (Fig. 3C). In most cases, ohnologs maintained in post-WGD species showed a strong asymmetry of PPIs, where one copy of the post-WGD ohnolog pair has lost most of its PPIs (Fig. 3D). In *N. castellii*, most PPIs were maintained for the ohnolog NCAS0D03820 (B), whereas NCAS0A01090 (a) only showed interactions with Ssa1p and Sba1p. These two proteins involved in protein folding are abundant proteins that are flagged as nonspecific interactors in DHFR-PCA screens and that are used as abundance controls (Tarassov et al. 2008). Detecting these interactions confirmed the protein level expression of ohnologs, even for copies that did not complement in our assays. These analyses strongly support the previous results that many of the faster evolving ohnologs are on their way to nonfunctionalization as they lost

many functions related to their interaction with other proteins.

One exception that could potentially show divergence of function is ohnologs maintained in *K. africana*, which showed ohnolog-specific PPIs. Such PPIs were in some cases not observed for non-WGD orthologs or the *S. cerevisiae* ortholog. These could be cases of interactions that evolved in this species since the WGD event. Among all ohnolog-specific PPIs, we focus on interactions that have similar molecular functions. We observed two such cases, Pex11p/Pex19p/Pex30p and Myo2p/Myo3p/Myo5p (Fig. 3D). In the case of Pex11p/Pex19p/Pex30p interactions, we observed both ohnologs interacting with Pex19 as in non-WGD orthologs, whereas ohnologs KAFR0C02290 (B) and KAFR0K00320 (A) separately gained interactions with Pex11p and Pex30p, respectively. Pex11p, Pex19p, and Pex30p are proteins involved in the peroxisome biogenesis. While Pex19p plays a role in the docking of the receptor-cargo protein complex on the peroxisome membranes, Pex30p and Pex11p are involved in distinct timing and processes of the peroxisome biogenesis pathway. More specifically, Pex30p localizes to the endoplasmic reticulum (ER), enriched at the site of pre-peroxisome vesicle formation, and regulates the tubular structure. Pex11p is responsible for membrane elongation of preexisting peroxisomes (Deori and Nagotu 2022). Since non-WGD orthologs show interactions with some of these proteins, the detection of specific PPIs for KAFR0C02290 (B) and KAFR0K00320 (A) with them may indicate slight changes of function.

In the case of Myo2p/Myo3p/Myo5p interactions, we observe that the ohnolog KAFR0K00320 (A) interacts with Myo3p/Myo5p as non-WGD orthologs do, while the other ohnolog KAFR0C02290 (B) has lost the interaction with Myo3p/Myo5p and gained interaction with Myo2p, which was not detected for any of the non-WGD orthologs. Myo2p, Myo3p, and Myo5p are myosin motor proteins, and they are involved in actin-based cargo transport and endo/exo-cytosis in actin cortical patches, respectively (Tanaka and Matsui 2001). Myo3p and Myo5p contain a Src homology 3 (SH3) domain, which contributes to PPIs by recognition of binding motifs (Tonikian et al. 2009; Dionne et al. 2021). The SH3 domains in Myo3p and Myo5p are required for targeting to sites of actin polarization (Anderson et al. 1998). Interestingly, Myo2p is also an ohnolog (with Myo4p) so this change in PPIs could have evolved since the WGD. When focusing on other PPI partners containing SH3 domains, we found that Lsb3p and Sla1p gained and lost PPIs in some orthologs, respectively.

PPIs with SH3 domains are achieved through protein binding motifs, leading us to examine the sequence difference in orthologs that contribute to the gain and loss of PPIs with SH3 domain-containing proteins. We examined the presence of SH3 binding motifs in Hrr25p orthologs for the SH3 domain-containing proteins of which we observed at least one interaction in this study. To identify the SH3 binding motifs, we used position weight matrices



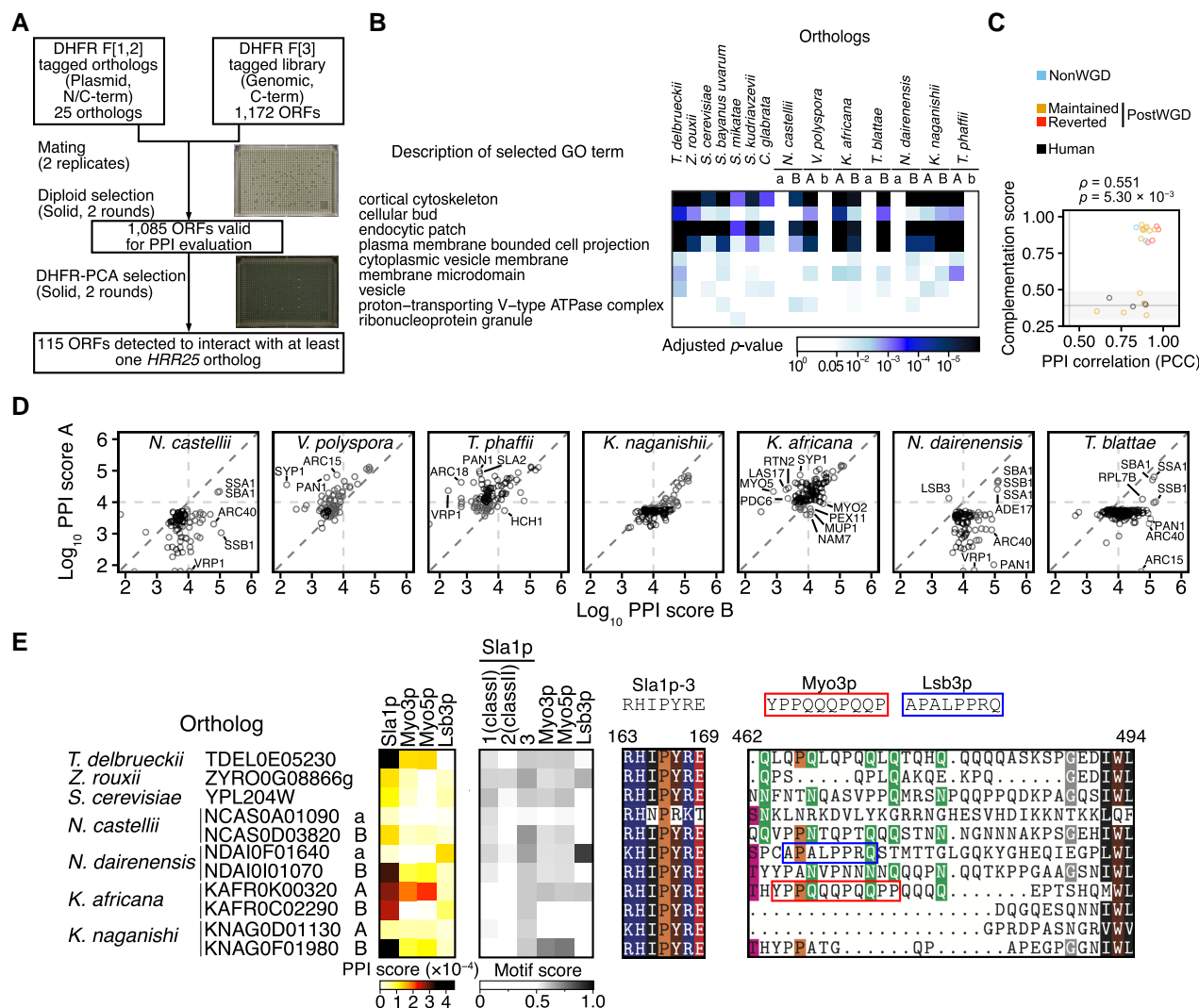


**Fig. 3.** Protein interaction profiles of Hrr25p orthologs with the *S. cerevisiae* proteome. **A**) Experimental workflow for proteome-wide PPI screening. *HRR25* orthologs were cloned into CEN/ARS plasmids and screened against the proteome-wide genomically tagged DHFR F[3] collection by DHFR-PCA. Typical plate images of endpoints are shown for diploid selection and PPI selection. **B**) Heatmap representation of GO enrichment of detected PPIs for each ortholog. GO terms with the same descriptions were grouped. Lowest values for each GO term description were used for visualization. GO terms with redundant terms are not shown in this figure. See [supplementary table S7, Supplementary Material](#) online for detailed description and raw data. **C**) Correlation between PPI profile similarity with *S. cerevisiae* and functional complementation scores. PPI profile similarity values are Pearson correlation coefficients of a given ortholog versus the *S. cerevisiae* ortholog using the PPI score of 115 PPI partners. The gray line and shaded area indicate mean and 95% confidence interval for the vehicle (empty plasmid), respectively. Values for *S. cerevisiae* were excluded from this analysis. Pearson correlation ( $\rho = 0.551$ ,  $P$ -value =  $5.03 \times 10^{-3}$ ). **D**) Scatter plot of PPI scores for maintained orthologs pairs in post-WGD species. Horizontal and vertical dashed lines represent thresholds to call positive interactions. The diagonal line represents equal PPI scores for both orthologs. **E**) PPI profiles for selected orthologs on SH3-encoding protein interaction partners which showed loss or gain of PPIs. Left: Heatmap representation of PPI scores. Middle: Heatmap representation of motif scores for each binding motif within orthologs. Right: Multiple sequence alignment (MSA) of binding regions for Sla1p, Myo3p, and Lsb3p. Binding motifs within the region are indicated above the MSA. Protein positions for *S. cerevisiae* (total length of 494) are shown above the MSA.

(PWMs) constructed from quantitative motif binding assays (Tonikian et al. 2009). We examined the occurrence of PWM matches within each ortholog (MSS; matrix similarity score), and used the highest value as the motif score (see the Materials and Methods section for details). We found that the *K. africana* ortholog, KAFR0C02290 (B), which lost interactions with Sla1p, Myo3p, and Myo5p has acquired mutations contributing to the decrease of motif score for the corresponding binding partners. In

contrast, the *N. dairenensis* ortholog NDAI0F01640 (a), which gained interaction with Lsb3p, has accumulated mutations which increased the motif score for the Lsb3p binding motif (Fig. 3E).

Taken together, while neofunctionalization and/or subfunctionalization at the GO term level were not observed, we observed instances of gain of specific PPIs in two separate biological processes for some Hrr25p post-WGD orthologs. In both of these cases, the gained interaction partners were



functionally related to interactors of non-WGD orthologs. These cases could represent cases of neofunctionalization in the classical sense (Ohno 1970). The potential adaptive significance of these changes remains to be investigated.

### Noncomplementing Ohnologs Have Abnormal Subcellular Localization

Hrr25p is known to require both kinase activity and PPIs for its functionality. For example, the central domain of Hrr25p interacts with Mam1p, localizing Hrr25p to the meiosis I centromeres (Ye et al. 2016). In this case, both kinase activity and Mam1p binding are essential for monopolar attachment of Hrr25p, shown from abnormal chromosome segregation when mutations in the kinase domain (H25R and E34K) are introduced (Petronczki et al. 2006). Mutations that disrupt the kinase function also cause abnormality in localization for the human CK1δ (CSNK1D) (Milne et al. 2001). Another example is the localization of Hrr25p to cytoplasmic RNP granules (P-bodies) under stress conditions and during meiosis. The localization of Hrr25p to P-bodies protects this enzyme from the degradation machinery during these periods of stress (Zhang et al. 2016). The PLS in the central domain mediates the interaction between Dcp2p and allows Hrr25p to localize to the P-body. This localization at the P-body foci is also seen for the human CK1δ (CSNK1D) in HeLa cells (Zhang et al. 2016). While kinase activity is required for P-body localization of Hrr25p, the mutations that cause deficiency in monopolar attachment (H25R and E34K) do not affect localization to P-body foci or sporulation efficiency (Zhang et al. 2018). Collectively, these observations indicate that the diverse functions of Hrr25p are achieved through localization that depends on kinase activity and PPIs.

We examined the localization of each ortholog using an mEGFP reporter (supplementary fig. S3, Supplementary Material online). The *S. cerevisiae* Hrr25p showed localization similar to previous observations, localizing to the budneck, cytoplasm, nucleus, and the bud (Ghaemmamghami et al. 2003). The orthologs from non-WGD species, *Z. rouxii* and *T. delbrueckii*, showed similar localization patterns to the *S. cerevisiae* Hrr25p, again showing that this is likely the ancestral localization. The localization of complementing ohnologs also showed similar patterns to that of the *S. cerevisiae* Hrr25p. On the other hand, consistent with the complementation assays, noncomplementing ohnologs did not show localization to the budneck, but instead showed localization in foci in the cytoplasm, while the *T. blattae* ortholog TBLA0A02040 (a) showed exclusive localization to the nucleus, similar to the report for the catalytic dead human homolog (Milne et al. 2001). The localization of orthologs therefore largely agrees with our observations on functional complementation and PPIs.

### One Ohnolog Appears on its way to Nonfunctionalization in *N. castellii*

We have shown that many HRR25 ohnologs in post-WGD species underwent asymmetrical evolution and lost the

ability to complement the essential function of this kinase in *S. cerevisiae*. These results suggest that one gene within many of the ohnolog pairs is on its way to nonfunctionalization. One striking case is the *N. castellii* ohnolog NCAS0A01090 (a) compared with its ohnolog NCAS0D03820 (B). Sequence level analysis has shown that this ohnolog has evolved faster than the other, likely due to relaxed selection. This ortholog failed to complement the loss of HRR25 in *S. cerevisiae*, lost most of the PPIs we observed, and showed abnormal subcellular localization. Changes in the kinase domain of NCAS0A01090 (a) specifically appear to be causing these losses of function.

These observations led us to hypothesize that HRR25 orthologs in post-WGD species are evolving under the dosage subfunctionalization model (Gout and Lynch 2015), where decrease in gene expression promotes nonfunctionalization of one ohnolog by relaxing selection on its function. We first examined the expression level of HRR25 orthologs across non-WGD and post-WGD species. We compared expression from *S. cerevisiae* (post-WGD, single copy reverted), *N. castellii* (post-WGD), and *Kluyveromyces lactis* (non-WGD), and normalized the data based on common 1:1 orthologs to be able to directly compare transcript levels among species, as done in Qian et al. (2015). Based on available data, we observed that HRR25 expression levels in *S. cerevisiae* and *K. lactis* are slightly above the mean of 1:1 orthologs (Log<sub>2</sub> fold-change of 0.568 and 0.140, respectively). In *N. castellii*, the complementing ohnolog NCAS0D03820 (B) has a similar level of expression to the mean 1:1 orthologs (Log<sub>2</sub> fold-change = −0.035) (Fig. 4A). In contrast, the ohnolog NCAS0D03820 (a) has a lower expression level, with a Log<sub>2</sub> fold-change of −2.154 relative to the mean of 1:1 orthologs. We examined how this difference in expression compares with the divergence of expression of other ohnolog pairs and found that the expression difference between NCAS0A01090 (a) and NCAS0D03820 (B), a 5-fold difference in expression, is at the 70th percentile in expression asymmetry among all WGD duplicate pairs in this species (Fig. 4B and C). Interestingly, a >5-fold difference in expression was previously shown to cause an asymmetry of mutational effects, where new nonsynonymous mutations and frameshift-causing indels are significantly more deleterious in the highly expressed copy compared with their paralogs with lower expression (Johri et al. 2022), which is consistent with our observation of nonfunctionalization.

To validate our finding that NCAS0A01090 (a) has lost the ancestral essential function and is likely undergoing nonfunctionalization, we tested the essentiality of these two *N. castellii* ohnologs *in vivo*. We knocked out the orthologs in *N. castellii* and performed tetrad dissections to assess spore viability. As a result, tetrads with the NCAS0A01090 (a) knockout but not the NCAS0D03820 (B) knockout were viable, indicating that NCAS0A01090 (a) has become dispensable in *N. castellii* (Fig. 4D). The imbalance of essentiality demonstrates that the ancestral essential functions of HRR25 are maintained only in NCAS0D03820 (B), but have been lost for NCAS0A01090 (a).

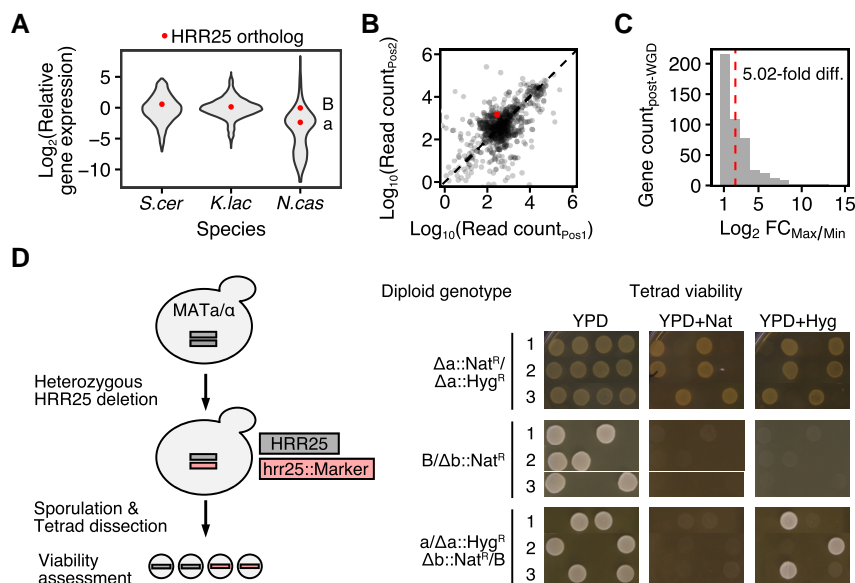


**Fig. 4.** Validation of the loss of essential function for *N. castellii* NCAS0D03820. **A)** *HRR25* mRNA abundance in *S. cerevisiae*, *K. lactis*, and *N. castellii*. Violin plots represent the distribution of gene expression levels in each species. Expression values were normalized based on mean expression levels of 1:1 orthologs present in all three species. Red points indicate the *HRR25* orthologs in each species. *N. castellii* ohnologs are annotated as (a) (NCAS0A01090) and (b) (NCAS0D03820). **B)** Scatter plot representation of gene expression for post-WGD ohnolog pairs in *N. castellii*. Each point represents one ohnolog pair, with raw read counts retrieved from GSE90041. The diagonal line represents equal expression between ohnolog pairs. The red point denotes *HRR25* ohnologs. The axes (Pos1 and Pos2) are interchangeable for each point and do not reflect any meaning for the encoded loci. **C)** Distribution of gene expression imbalance for post-WGD ohnolog pairs in *N. castellii*.  $\log_2$  fold-change was computed for each WGD ohnolog pair by taking the ratio of read counts between the most highly expressed (Max) and the other (Min) ohnolog. The red dashed line represents the value for the *HRR25* ohnologs, with a fold change value of 5.02. **D)** Tetrad dissection analysis in *N. castellii* for assessing the essentiality of each *HRR25* ohnolog. (Left) Illustration of the experimental procedure. Diploid *N. castellii* strains were used to construct strains carrying heterozygous deletion of *HRR25* ohnologs. Strains were then sporulated and tetrads were dissected for assaying the viability of each genotype using selection markers. (Right) Spot assay for tetrad viability. Three diploid strains were subjected for this analysis. Each row represents a different tetrad. Three of the typical tetrads are shown. *HRR25* loci are annotated as (a) NCAS0A01090 and (b) NCAS0D03820.

## Conclusion

In this study, we investigated the fate of *HRR25* using orthologs from 12 species descending from the same WGD event. We asked which of the evolutionary scenarios (subfunctionalization, neofunctionalization, or nonfunctionalization) could explain the retention of *HRR25* duplicates in many of these species. Sequence level analysis showed that *HRR25* in species which maintain both ohnologs is under more relaxed selection compared with orthologs of non-WGD or single copy reverted post-WGD species. Functional complementation assays showed that when ohnologs are evolving asymmetrically, the faster evolving ohnolog fails to complement the function of the *S. cerevisiae* *HRR25*. A proteome-wide PPI screening against *S. cerevisiae* proteins showed similar patterns at the molecular level, where orthologs evolving faster than other orthologs have lost most of their PPIs. We validated our findings in *N. castellii* and showed that the faster evolving ohnolog has become dispensable in this species. The fact that this dispensable copy has much lower expression level *in vivo* supports its potential decreased functionality. Taken together, our results indicate that many *HRR25* orthologs could be nonfunctionalizing, likely following the dosage subfunctionalization model (Gout and Lynch 2015), whereby asymmetry in expression leads to relaxed

selection on one ohnolog and then to its slow degeneration at the protein level. This model does not apply to all WGD species. For instance, in some species where both ohnologs of *HRR25* appear more conserved, we discovered potentially recently gained PPIs, which may suggest neofunctionalization of some ohnologs that is supported by the coincidental evolution of SH3 domain-binding motifs. Such gain of PPIs may represent early states of neofunctionalization in the classical sense (Ohno 1970). The contribution of these gained PPIs to biological functions and/or adaptive significance remains to be explored.

We recognize the limitations of our work, namely, because all other species are not amenable to similar assays, complementation and PPI assays were performed in *S. cerevisiae*. The complementation assays could only reveal results related to the essential functions of the *S. cerevisiae* ortholog and not other functions that could have evolved in other species. This is also the case for PPIs. In addition, the co-evolution of the PPI partners within species could lead to losses of interactions in *S. cerevisiae* even if PPIs are maintained within the other species. However, this would be unlikely to occur at the scale of the entire interactome.

The support to our conclusions comes from the combination of various observations made based on the rates

of evolution and the assays we performed. *HRR25* represents a rare case of maintenance of ohnolog pairs in many post-WGD species and as such, it could be an exceptional representative of pairs that are destined to return to single copy but that have not completed the process yet. One potential question that our results lead to is, given the ease with which mutations can lead to complete loss of function of genes, for instance through indels and stop codons, why are *HRR25* ohnologs sequences still largely intact? One potential answer is that the dosage subfunctionalization model leads to a slow decay of gene functions as changes in expression and coding sequences slowly reinforce each other. By reducing the expression level of one ohnolog, early regulatory mutations could have reduced the strength of selection acting on the coding sequence, leading to the accumulation of degenerative mutations that would have been deleterious in the ancestral copy or in the other ohnolog. A less functional protein would then contribute less to function, potentially lessening selective pressures on expression level on this ohnolog. This feedback cycle will eventually lead to gene loss being effectively neutral (Gout and Lynch 2015). Before effective neutrality is attained, mutations with drastic negative effects could still be selected against.

There are two factors that could have caused *HRR25* to undergo this process in a very slow manner. The first is the dosage constraint acting on *HRR25*, which is reported to be critical during meiosis in *S. cerevisiae* (Zhang et al. 2018). While it was not examined in our experimental conditions, the fact that lower *HRR25* levels could negatively impact sexual reproduction may have positively influenced the maintenance of both duplicates. Another factor is the multifunctional nature of the *HRR25*. Since there are numerous functions that this kinase participates in, the non-functionalizing copy could keep partial functions but that are not essential. This was observed from our results where the nonfunctionalizing copy maintained/gained some PPIs. The combination of these factors may select against complete loss of function mutations because there is still some contribution to fitness.

## Materials and Methods

### Ortholog Sequence Retrieval

We first extracted protein sequences of Hrr25p for species in the *Saccharomycetaceae* from the NCBI RefSeq database (<https://www.ncbi.nlm.nih.gov/refseq>, last accessed 2023 September 18). Among the 91 RefSeq genomes available in NCBI, 34 species had RefSeq protein files available. We performed a protein–protein BLAST (blastp, version 2.6.0+) (Altschul et al. 1990) using the *S. cerevisiae* Hrr25p as a query, with an *e*-value threshold of  $1e-10$ . Two hundred and six proteins were identified from this search. These proteins were subsequently aligned to all *S. cerevisiae* proteins to evaluate false positives. Among the 206 proteins, 46 proteins from 34 species aligned with Hrr25p as their best hit.

We used the phylogenetic tree from Li et al. (2021) as the species reference tree. We trimmed this species tree based on the species from which the *HRR25* protein sequences were retrieved, using the `tree_subset` function of the R package `treeio` (Wang et al. 2020). For additional species which were not included in our first criteria but present in the trimmed tree, genome sequences were retrieved from the NCBI database and from Shen et al. (2018). *HRR25* orthologs were identified by aligning orthologs from the first criteria to the genomic sequences using BLAST (blastn, version 2.6.0+) (Altschul et al. 1990), followed by precise extraction of *HRR25* loci based on a global alignment using MAFFT (version 7.392) with the L-INS-i method (Katoh and Standley 2010). We manually checked the resulting dataset and observed that in some species not all orthologs had been retrieved due to low genomic coverage, as seen from orthologs partially aligning to the edge of contigs. We therefore excluded *Kazachstania* species with only one *HRR25* ortholog identified for further analysis, eliminating single copy reversion annotations which are not reflecting actual events. The annotated sequences of *N. castellii* orthologs in the type strain CBS 4309 (Wolfe et al. 2015) were validated by Sanger sequencing. The details of genes used in this analysis are shown in [supplementary table S1, Supplementary Material](#) online.

### Multiple Sequence Alignment Analysis

The global multiple sequence alignment of *HRR25* orthologs was performed using MAFFT (version 7.392) with the L-INS-i method (Katoh and Standley 2010). A custom script was used to evaluate the residue similarity against the non-WGD ortholog of *T. delbrueckii*. For each of the orthologs, we obtained the similarity score for each residue using the BLOSUM62 similarity matrix (Henikoff and Henikoff 1992). Indels were assigned a score of  $-10$  for this analysis. We computed the normalized relative conservation score of each residue by dividing the similarity score with that of an identical match against *T. delbrueckii*, and multiplied this value by 100.

### *dN/dS* Analysis

We constructed a reconciled gene tree using the species tree from Li et al. (2021) and replaced the WGD clade using the gene tree of post-WGD orthologs. The gene tree for post-WGD duplicates were created following the tutorial paper by Álvarez-Carretero et al. (2023), using codon-based alignment using TranslatX (Abascal et al. 2010) and RAXML-NG (Kozlov et al. 2019). For the *dN/dS* analysis, we eliminated aligned positions which were not present in >90% of orthologs. The *dN/dS* values were computed using the `codeml` program in the PAML package (version 4.10.6, last accessed 2023 September 18 at <https://github.com/abacus-gene/paml>) (Yang 2007). The homogenous and branch models were used. For domain specific computation of *dN/dS*, we separately executed the `codeml` program using the branch model on each of



the three protein domains. Domains for each ortholog were inferred from alignment to the *S. cerevisiae* HRR25, where the MSA positions are defined as kinase domain (1 to 290), central domain (291 to 394), and the disordered tail region (395 to 898). Evolutionary rates were referred to the branch lengths of the *dN* tree output from the codeml program. Distances between nodes were calculated using the `get_all_pairwise_distances` function of the R package *castor* (version 1.7.11) (Louca and Doebeli 2019).

### List of Strains and Plasmids Used in This Study

The details of biological resources used in this study are listed in [supplementary table S2, Supplementary Material online](#).

### Oligonucleotides and Gene Fragments Used in This Study

Oligonucleotides and gene fragments used in this study are listed in [supplementary table S3, Supplementary Material online](#).

### Yeast Medium

YPD medium (1.0% yeast extract, 2.0% peptone, 2.0% dextrose) was used for general yeast cultures and complementation assays. We used buffered SC medium at pH 6.0 (amino acid dropout mix, 2.0% glucose, 0.1% monosodium glutamate, 1% succinic acid, and 0.6% NaOH) for yeast cultures for Western blotting and microscopy experiments. Antibiotics were supplemented in final concentrations of G418: 200 µg/mL, CloNAT (NAT): 100 µg/mL, Hygromycin B (HPH): 250 µg/mL, and doxycycline (DOX): 10 µg/mL, unless otherwise stated.

### Strain Constructions for Combinatorial Functional Complementation Assay

The background strain R1158 was used for constructing the DOX inducible repressor strain (Horizon discovery, YSC1210) (Hughes et al. 2000). In order to enable efficient combinatorial screenings via mating, we constructed a BY4742-derived MAT $\alpha$  strain for constructing DOX repressor strains. We achieved this by amplifying the URA3::CMV- $\tau$ TA cassette from R1158 using primers CLO1-6 and CLOP167-D11. Amplification was performed using Q5 High-Fidelity DNA Polymerase (New England Biolabs, M0491L). The polymerase chain reaction (PCR), in a final volume of 25 µL, consisted of 1× Q5 reaction buffer, 200 µM of dNTPs, 500 nM of each forward and reverse primer, 0.5 unit of Q5 polymerase, and 200 ng of template genomic DNA. Thermal cycling conditions were (i) 98 °C for 30 s; (ii) 35 cycles of 98 °C for 10 s, 64 °C for 10 s, and 72 °C for 4 min; (iii) 72 °C for 10 min; and (iv) 12 °C forever. We integrated this cassette to the URA3 locus of BY4742 by homologous recombination using standard lithium acetate transformation and selected the successful transformants on SC-Ura plates. The resulting strain yPE014 was subjected to genotyping PCR for confirmation using the same conditions as above.

### Plasmid Construction for Tet-Off Repressor Strain Construction

For efficient construction of TetO<sub>7</sub> promoter-tagged strains, we created a plasmid, pKB33, having the KanMX-TetO<sub>7</sub> cassette (Hughes et al. 2000) in the cloning vector pUC19. We amplified the genomic region encoding the KanMX-TetO<sub>7</sub> from R1158-derived yTHC4703 (Horizon Discovery, YSC1180) using primers CLOP258-A6 and CLOP258-B6, and inserted it into the pUC19 digested with restriction enzymes SacI-HF (New England Biolabs, R3156) and XbaI (New England Biolabs, R0145S) by *in vitro* DNA assembly (Gibson et al. 2009). This product was transformed into chemically competent *Escherichia coli* strain MC1061 and selected on 2YT + Amp plates. The construct was validated using genotyping PCR followed by Sanger sequencing of the inserted region.

### Tet-Off Repressor Strain Construction

The KanMX-TetO<sub>7</sub> cassette on the plasmid pKB33 was PCR amplified with primers CLOP280-C5 and CLOP280-D5 having homology to replace the promoter region of HRR25. Amplification was performed using Kapa HiFi Hotstart Polymerase (Roche, 07958897001). The PCR reaction, in a final volume of 25 µL, consisted of 1× reaction buffer, 300 µM of dNTPs, 300 nM of each forward and reverse primer, 0.5 unit of polymerase, and 1 ng of template DNA. Thermal cycling conditions were (i) 95 °C for 5 min; (ii) 35 cycles of 98 °C for 20 s, 60 °C for 15 s, and 72 °C for 1:45 min; (iii) 72 °C for 3:30 min; and (iv) 12 °C forever. The resulting PCR product was used for genomic integration of yeast strains R1158 and yPE014, and plated on YPD + G418 plates for successful transformants. Insertion of the KanMX-TetO<sub>7</sub> cassette was confirmed by genotyping PCR using primers CLOP280-A5 and CLOP280-B5 using thermal cycler conditions as described above. We named the R1158-derived MAT $\alpha$  strain GS007 and the yPE014-derived MAT $\alpha$  strain GS009.

### Gene Synthesis and ENTRY Clone Preparation for Gateway Cloning

We amplified the *S. cerevisiae* HRR25 from genomic DNA of BY4741 using primers CLOP280-E5 and CLOP280-F5 to add the attB sites for Gateway BP reactions. Amplification was performed using Kapa HiFi Hotstart Polymerase (Roche, 07958897001). The PCR reaction, in a final volume of 25 µL, consisted of 1× reaction buffer, 300 µM of dNTPs, 300 nM of each forward and reverse primer, 0.5 unit of polymerase, and 4 ng of template DNA. Thermal cycling conditions were (i) 95 °C for 5 min; (ii) 30 cycles of 98 °C for 20 s, 60 °C for 15 s, and 72 °C for 1 min; (iii) 72 °C for 3:30 min; and (iv) 12 °C forever. For orthologous genes, we focused on species present in the YGOB database (Byrne and Wolfe 2005), with available RefSeq protein records. Protein sequences of orthologs were retrieved from the RefSeq protein files, and DNA fragments were synthesized (TWIST biosciences).

All DNA fragments were codon optimized for expression in *S. cerevisiae*, and attB sequences were added for Gateway BP cloning. For genes which exceeded the synthesis limit (TBLA0A02040 and NDAI0F01640), we added the attB sites via PCR. PCR reactions were performed using the same conditions as described above. Primer information are listed in [supplementary table S3, Supplementary Material](#) online. We individually subcloned the *HRR25* orthologs to pDONR201 by Gateway BP cloning (Invitrogen, 11789), following the manufacturer's instructions. This product was transformed to chemically competent *E. coli* strain DH5α and selected on LB + Kan plates. The constructs were validated by Sanger sequencing. The human orthologs were retrieved from the CCSB human ORFeome resource version 8.1 ([Rual et al. 2005](#)) and were validated by Sanger sequencing. The details of the genes used in this study are shown in [supplementary table S1, Supplementary Material](#) online.

### Construction of Destination Vectors for Functional Complementation Assays

We constructed Gateway compatible destination vectors for ORF expression in two steps. First, we constructed pDN0520, an expression plasmid with an auxotrophic TRP1 marker by eliminating the DHFR F[1,2] region of pDN0509 ([Marchant et al. 2019](#)). This was achieved by inserting a synthesized dsDNA fragment dsOPE001 into the SpeI (New England Biolabs, R3133S) and I-SceI (New England Biolabs, R0694S) digested pDN0509 backbone, by ligation. Ligation reactions were performed using T4 DNA ligase (New England Biolabs, M0202S) following the manufacturer's instructions. The ligated product was transformed to One Shot ccdB Survival 2 T1<sup>R</sup> Competent Cells (Invitrogen, A10460) and selected on LB + Amp plates. The construct was validated using restriction enzyme digestion, followed by Sanger sequencing. We then replaced the backbone containing the marker with CloNAT and Hygromycin resistance to create pDN0603 and pDN0604, respectively. This was achieved by first digesting pDN0520 with I-SceI (New England Biolabs, R0694S), I-CeuI (New England Biolabs, R0699S), and SapI (New England Biolabs, R0569S) to obtain the ADH1pr-Gateway cassette. SapI was used to fragment the backbone, unnecessary for subsequent cloning. The insert region was then ligated to pKB11 and pKB12 (see the Construction of destination vectors for DHFR-PCA assays section) which were also treated with I-SceI and I-CeuI, giving the backbones with CloNAT and Hygromycin resistance cassettes, respectively. The backbones of pKB11 and pKB12 were treated with calf intestinal alkaline phosphatase (CIP) (New England Biolabs, M0525S) to prevent self-ligation. Ligation reactions were performed using T4 DNA ligase (New England Biolabs, M0202S) following the manufacturer's instructions. These products were transformed to chemically competent *E. coli* strain DB3.1 and selected on LB + Amp plates. The constructs were validated using restriction enzyme digestion, followed by Sanger sequencing.

### Strain Construction for Functional Complementation Assay

We individually subcloned *HRR25* orthologs into pDN0603 (pDEST-ADH1pr Nat<sup>R</sup>) and pDN0604 (pDEST-ADH1pr Hyg<sup>R</sup>) by Gateway LR cloning (Invitrogen, 11791), following the manufacturer's instructions. Expression vectors in pDN0603 and pDN0604 backbones were used to transform strains GS007 and GS009, respectively. Successful transformants were selected on YPD plates with appropriate antibiotics for selection.

### Functional Complementation Assay by Spot Assay

We mated the GS007 and GS009 strains with the vehicle and *S. cerevisiae* *HRR25* plasmids. Diploids were selected on YPD + NAT + HPH plates. We cultured haploid (GS007 or GS009) and diploid (GS007/GS009) strains carrying plasmids in 3 mL of YPD medium containing antibiotics for plasmid selection, for approximately 18 h at 30 °C with agitation. Spots were plated on YPD or YPD + DOX in 5-fold serial dilutions, starting from OD<sub>600 nm</sub> = 0.5.

### Combinatorial Functional Complementation Screening

The 52 haploid strains (26 baits and 26 preys) with plasmids were used to perform the complementation screening on a robotically manipulated pin tool (BM5-SC1, S&P Robotics Inc.). First, the preys (GS009 strains with pDN0604-ortholog constructs) were cherry-picked from 96-well plates to omnitrays in a 384 format on YPD + HPH solid media. Plates were then combined into the 1,536 format on YPD + HPH plates. The prey array comprised a border of control strains of 2 rows and 2 columns of BY4743, and 26 preys (25 *HRR25* orthologs and vehicle control) each with 9 or more replicates on random assigned positions. The border strains and the random position assignment of preys were used to minimize the effect of plate position. Second, baits (GS007 strains with pDN0603-ortholog construct) were grown in 10 mL of liquid YPD + NAT, and used to create a "lawn," which we prepared by transferring the overnight culture of bait strains on solid YPD + NAT omnitrays, and removed excess medium after letting the cells settle by waiting for approximately 3 min. The plates were dried and incubated at 30 °C for 48 h. They were then used to perform mating in 1,536 array format. Mating of baits with preys was done on YPD followed by incubation at 30 °C for 48 h. Two diploid selection steps were performed by replicating the plates on YPD + NAT + HPH and incubating them for 48 h at 30 °C. Pictures were taken at the end of the second diploid selection for quality control. All images were acquired with a EOS Rebel T5i camera (Canon). Finally, the diploid cells were replicated to YPD and YPD + DOX media for selection. The plates were incubated for 2 d as first round selection in a splmager custom robotic platform (S&P Robotics Inc.). Cells were replicated for 2 more rounds on each medium to reduce background for selection and incubated in the same manner. Pictures were taken every 2 h for the second and third selection for 3 d. The acquired images were

processed to obtain colony areas for each time point using pyphe version 0.981 using the pyphe-quantify function (Kamrad et al. 2020). The area under curve (AUC) was computed from the growth curve using colony areas using the trapz function of the numpy library version 1.24. Complementation scores were computed by taking the ratio of AUC values between nonselection (YPD) and selection (YPD + DOX). The AUC values and complementation scores for all constructs are shown in [supplementary table S4, Supplementary Material](#) online.

### Functional Complementation Assay of Chimeric Orthologs

The chimeric orthologs were constructed from expression vectors of orthologs in the pDN0603 backbone, namely pDN0603-HRR25 (*S. cerevisiae*), pDN0603-NCAS0A01090 (a) (*N. castellii*), and pDN0603-NCAS0D03820 (B) (*N. castellii*). We PCR amplified the kinase region (corresponding positions 1 to 290 in *S. cerevisiae* HRR25) of each construct with the backbone region, to produce each construct without the central/tail regions of the ortholog. Amplification was performed using Kapa HiFi Hotstart Polymerase (Roche, 07958897001). The PCR reaction, in a final volume of 25  $\mu$ L, consisted of 1 $\times$  reaction buffer, 300  $\mu$ M of dNTPs, 300 nM of each forward and reverse primer, 0.5 unit of polymerase, and 4 ng of template DNA. Thermal cycling conditions were (i) 95  $^{\circ}$ C for 5 min; (ii) 30 cycles of 98  $^{\circ}$ C for 20 s, 60  $^{\circ}$ C for 15 s, and 72  $^{\circ}$ C for 1 min; (iii) 72  $^{\circ}$ C for 1:30 min; and (iv) 12  $^{\circ}$ C forever. We PCR amplified the central/tail regions of these orthologs with homology to other kinase domains and the backbone. Amplification was also performed using Kapa HiFi Hotstart Polymerase (Roche, 07958897001). The PCR reaction, in a final volume of 25  $\mu$ L, consisted of 1 $\times$  reaction buffer, 300  $\mu$ M of dNTPs, 300 nM of each forward and reverse primer, 0.5 unit of polymerase, and 4 ng of template DNA. Thermal cycling conditions were (i) 95  $^{\circ}$ C for 5 min; (ii) 30 cycles of 98  $^{\circ}$ C for 20 s, 60  $^{\circ}$ C for 15 s, and 72  $^{\circ}$ C for 10 min; (iii) 72  $^{\circ}$ C for 15 min; and (iv) 12  $^{\circ}$ C forever. To construct each of the desired chimeric orthologs, the backbone (with the kinase domain) and the fragment containing central/tail regions were subjected to *in vitro* DNA assembly (Gibson 2009). The resulting products were transformed to chemically competent *E. coli* strain DH5 $\alpha$  and selected on LB + Amp plates. Constructs were validated by Sanger sequencing of the inserted region. Primers used to amplify each fragment are listed in [supplementary table S3, Supplementary Material](#) online. The plasmids encoding chimeric orthologs together with controls were transformed to GS007 using standard lithium acetate transformation and selected on YPD + NAT. The spot assay was performed as described in the Functional complementation assay by spot assay section.

### Molecular Visualization

The protein crystal structure of Hrr25p (PDB: 5CYZ) (Ye et al. 2016) was visualized using ChimeraX (version 1.5) (Pettersen et al. 2021).

### Plasmid Construction for Localization Assay

We constructed Gateway compatible destination vectors with C-terminal GFP fusion. This plasmid, pDN0617 (pDEST-Gateway-GFP Nat<sup>R</sup>), was constructed by cloning the mEGFP to pDN0603 (pDEST-Gateway Nat<sup>R</sup>).

We first constructed pUG27-mEGFP-ENO1t-SpHIS5 by inserting mEGFP and ENO1 terminator fragments into pUG27 (Gueldener et al. 2002) using *in vitro* DNA assembly (Gibson et al. 2009). All 3 fragments were PCR amplified using the Kapa HiFi Hotstart Polymerase (Roche, 07958897001) and treated with 1  $\mu$ L (20 units) of DpnI (New England Biolabs, R0176L) for 1 h at 37  $^{\circ}$ C before being purified on magnetic beads. The backbone fragment was amplified from pUG27 using primers CLOP161-F8 and CLOP161-F9, with the thermal cycling conditions as (i) 95  $^{\circ}$ C for 5 min; (ii) 35 cycles of 98  $^{\circ}$ C for 20 s, 68  $^{\circ}$ C for 15 s, and 72  $^{\circ}$ C for 2 min; (iii) 72  $^{\circ}$ C for 3 min; and (iv) 12  $^{\circ}$ C forever. The mEGFP fragment was amplified from the plasmid F65V-34a-mEGFP using primers CLOP161-F10 and CLOP161-F12. The ENO1 terminator fragment was amplified from pYTK051 (Addgene Kit #1000000061 position E3) (Lee et al. 2015) using primers CLOP161-G1 and CLOP161-G2. Both the mEGFP and ENO1 terminator fragments were amplified using the following thermal cycling conditions (i) 95  $^{\circ}$ C for 5 min; (ii) 5 cycles of 98  $^{\circ}$ C for 20 s, 60  $^{\circ}$ C for 15 s, and 72  $^{\circ}$ C for 30 s; (iii) 30 cycles of 98  $^{\circ}$ C for 20 s, 72  $^{\circ}$ C for 45 s; (iv) 72  $^{\circ}$ C for 3 min; and (v) 12  $^{\circ}$ C forever. All PCR reactions, in a final volume of 25  $\mu$ L, consisted of 1 $\times$  reaction buffer, 300  $\mu$ M of dNTPs, 300 nM of each forward and reverse primer, 0.3 unit of polymerase, and 10 ng of template DNA. Five microliters of the *in vitro* DNA assembly reaction were transformed into MC1061 and plated on LB + Amp. Correct construction of the plasmid was confirmed by Sanger sequencing.

We then constructed pDN0617 by cloning the mEGFP fragment of pUG27-mEGFP-ENO1t-SpHIS5 into pDN0603. The mEGFP fragment with homology to the pDN0603 backbone was amplified from pUG27-mEGFP-ENO1t-SpHIS5 using primers CLOP286-A11 and CLOP286-B11. Amplification was performed using Kapa HiFi Hotstart Polymerase (Roche, 07958897001). The PCR reaction, in a final volume of 25  $\mu$ L, consisted of 1 $\times$  reaction buffer, 300  $\mu$ M of dNTPs, 300 nM of each forward and reverse primer, 0.5 unit of polymerase, and 0.4 ng of template DNA. Thermal cycling conditions were (i) 95  $^{\circ}$ C for 5 min; (ii) 30 cycles of 98  $^{\circ}$ C for 20 s, 60  $^{\circ}$ C for 15 s, and 72  $^{\circ}$ C for 1 min; (iii) 72  $^{\circ}$ C for 1:30 min; and (iv) 12  $^{\circ}$ C forever. The mEGFP insert was column purified after DpnI (New England Biolabs, R0176S) treatment, and subjected to *in vitro* DNA assembly (Gibson et al. 2009) with SpeI-HF (New England Biolabs, R3133S) digested pDN0603 as backbone. This reaction was transformed to chemically competent *E. coli* strain DB3.1 and selected on LB + Amp plates. The construct was validated using restriction enzyme digestion, followed by Sanger sequencing.

### Strain Construction for Western Blotting and Localization Assay

We individually subcloned HRR25 orthologs to pDN0617 (pDEST-Gateway-GFP Nat<sup>R</sup>) by Gateway LR cloning



(Invitrogen, 11791), following the manufacturer's instructions. Expression vectors in pDN0617 backbones were used to transform BY4741. Successful transformants were selected on YPD + NAT plates.

### Western Blotting

First, BY4741 strains carrying a plasmid with each ortholog tagged with GFP were grown overnight in SC complete medium + NAT. The next morning, cells were diluted to 0.15 OD<sub>600 nm</sub> and grown for 6 h to reach exponential phase (1 OD<sub>600 nm</sub>). From this culture, 12.5 OD<sub>600 nm</sub> units of cells were collected and frozen at −80 °C. Each pellet was resuspended in 250 µL lysis buffer (Complete Mini Protease inhibitor cocktail, Millipore-Sigma 11836153001) and glass beads were added to the suspension. The mixture was vortexed for 5 min on a Turbomix. After vortexing, 25 µL of 10% SDS was added to each tube and then boiled for 10 min. Tubes were then centrifuged at 16,000 × g for 5 min to clear the supernatant. Samples for SDS-PAGE gel were prepared by mixing 17.5 µL cell extract, 2.5 µL DTT 1M and 5 µL LB 5× (250 mM Tris-Cl pH 6.8, 10% SDS, 0.5% Bromophenol Blue, 50% glycerol). Samples were run on 8% SDS-PAGE gel for 1 h at 175 V (Tetra cell, BioRad). Following migration, proteins were transferred to a nitrocellulose membrane for 75 min at 0.8 mA/cm<sup>2</sup>. Once on the nitrocellulose membrane, proteins were stained with Ponceau Red to check for proper and uniform loading/transfer (Romero-Calvo et al. 2010). Following the imaging of the Ponceau Red staining, the membranes were blocked overnight in the blocking solution [Intercept (PBS) Blocking Buffer, 927-70003, Mandel Scientific] at room temperature with agitation. The next morning, membranes were soaked in blocking solution +0.02% Tween 20 with 0.15 µg/mL GFP antibody (Millipore-Sigma 11814460001) for 30 min. After the primary antibody incubation, the membranes were washed 3 times each for 5 min with PBS + T (10 mM sodium phosphate dibasic, 135 mM NaCl, 2 mM KCl, 1.5 mM monopotassium phosphate, 0.1% Tween 20). For the secondary antibody, the membranes were again soaked in blocking solution +0.02% Tween 20 with 0.075 µg/mL Anti-Mouse 800 (LIC-926-32210, Mandel Scientific) for 30 min. The membranes were washed another 3 times each for 5 min and then imaged with an Odyssey Fc instrument (Licor, Mandel Scientific) using the 700 and 800 channels.

### Construction of Destination Vectors for DHFR-PCA Assays

We constructed gateway compatible DHFR-PCA plasmids pKB11 (pDEST-DHFR F[1,2] C-term Nat<sup>R</sup>), pKB12 (pDEST-DHFR F[3] C-term Hyg<sup>R</sup>), pDN0605 (pDEST-DHFR F[1,2] N-term Nat<sup>R</sup>), and pDN0606 (pDEST-DHFR F[3] N-term Hyg<sup>R</sup>) to tag the genes of interest in the C-terminus and N-terminus, respectively. We first constructed pKB11 by replacing the TRP1 auxotrophic cassette of pDEST-DHFR F[1,2]-C (TRP1) (Addgene #177795) (Marchant et al. 2019) with the Nat<sup>R</sup> marker. We amplified the Nat<sup>R</sup> cassette using primers CLOP148-G1 and

CLOP148-G2 from pAG25 (Euroscarf, P30104). The backbone region without the auxotrophic marker was prepared by PCR amplification of pDEST-DHFR F[1,2]-C (TRP1), using primers CLOP157-H1 and CLOP157-H2. These insert and backbone fragments were subjected to *in vitro* DNA assembly to create pKB11. Correct construction of pKB11 was confirmed by Sanger sequencing. In a similar way, pKB12 was constructed by replacing the LEU2 auxotrophic cassette of pDEST-DHFR F[3]-C (LEU2) (Addgene #177796) (Marchant et al. 2019) with the Hyg<sup>R</sup> marker, using pAG32 (Euroscarf, P30106). The N-terminus fusion plasmids pDN0605 and pDN0606 were constructed using pDEST-DHFR F[1,2]-N (TRP1) and pDEST-DHFR F[3]-N (LEU2) (Addgene #177797 and #177798) (Evans-Yamamoto et al. 2022), and replacing the backbone region containing the selection marker with that of pKB11 and pKB12, respectively. This was achieved by restriction enzyme digestion followed by ligation. Both inserts and backbones were digested with I-SceI (New England Biolabs, R06945) and I-CeuI (New England Biolabs, R06995) homing endonucleases to obtain the ADH1pr-DHFR F[1,2]-Gateway cassette and backbone, respectively. The digested products of the backbone (pKB11 and pKB12) were treated with CIP (New England Biolabs, M0525S) to prevent self-ligation.

### DHFR-PCA Assay

We individually subcloned HRR25 orthologs to pKB11 (pDEST-DHFR F[1,2] C-term Nat<sup>R</sup>) and pDN0605 (pDEST-DHFR F[1,2] N-term Nat<sup>R</sup>) by LR cloning (Invitrogen, 11791), following the manufacturer's instructions. The plasmids were purified and used to transform BY4741 strains using standard lithium acetate transformation. The pKB11 and pDN0605 constructs were transformed into BY4741, and selected on YPD + NAT plates for successful transformants. We used these strains to test for interactions against the DHFR F[3] miniarray, in the BY472 background. The DHFR F[3] miniarray is a collection of strains with genomically fused 1,172 genes to the DHFR F[3] reporter in *S. cerevisiae*, which have been reported to have at least one PPI using DHFR-PCA (Tarassov et al. 2008; Rochette et al. 2015; Diss et al. 2017). The full list of proteins in the DHFR F[3] miniarray is shown in [supplementary table S5, Supplementary Material](#) online. DHFR-PCA screening was performed using a robotically manipulated pin tool (BM5-SC1, S&P Robotics Inc.) as previously described (Rochette et al. 2015).

First, the preys (DHFR F[3] miniarray collection) were grown on omnitrays in a 384 format on YPD + HPH solid media. Plates were then combined into the 1,536 format on YPD + HPH plates. The prey array comprised a border of control strains of 2 rows and 2 columns corresponding to the PPI between LSM8-DHFR F[1,2] and CDC39-DHFR F[3]. The presence of border strain and the random position assignment of preys were performed to minimize the effect of plate position. Second, baits (strains each carrying one of the HRR25 orthologs) were grown in 10 mL of liquid YPD + NAT and used to create a "lawn," which we

prepared by transferring the overnight culture of bait strains on solid YPD + NAT omnitrays, and removed excess medium after letting the cells settle by waiting for approximately 3 min. The plates were dried and incubated at 30 °C for 48 h. They were then used to perform the mating in 1,536 array format. Mating of DHFR F[1,2] baits with DHFR F[3] preys was done in 2 independent replicates on YPD followed by incubation at 30 °C for 48 h. Two diploid selection steps were performed by replicating the plates on YPD + NAT + HPH and incubating them for 48 h at 30 °C. Pictures were taken at the end of the second diploid selection for quality control. All images were acquired with a EOS Rebel T5i camera (Canon). Finally, the diploid cells were replicated on omnitrays containing solid PCA selection media and incubated for 4 d as a first selection step in a splmager custom robotic platform (S&P Robotics Inc.). Cells were replicated for a second PCA selection step and incubated in the same manner. Pictures were taken every 2 h for the second PCA selection for 4 d. The images were processed to obtain colony areas for each time point using pyphe version 0.981 using the pyphe-quantify function (Kamrad et al. 2020). The AUC was computed from the growth curve using the trapz function of the numpy library version 1.24. Colonies were quality filtered based on the colony area of the diploid selection plate, where colonies with  $\text{Log}_2$  transformed area below 10 were excluded for PPI evaluation. We set a threshold to call positive interactions at  $\text{AUC} = 1.0 \times 10^4$ , based on the distribution of AUCs among tested pairs. We note that, of the 2 tagging orientations (N-terminal and C-terminal tagging) tested for HRR25 orthologs, only the C-terminal tagged constructs showed interactions. Subsequent analyses were performed on the data generated from the C-terminal tagged constructs only. The PPI score data generated from the C-terminal tagged constructs are shown in [supplementary table S6, Supplementary Material](#) online.

### GO Enrichment Analysis of PPI Partners

PPI partners for each ortholog were classified according to their Gene ontology (GO) term as implemented in the enrichGO function of the R package clusterProfiler (Yu et al. 2012), using gene sets of cellular components in the *S. cerevisiae* database. *P*-values were adjusted using the Benjamini and Hochberg method. GO terms with the same description were combined and represented with the lowest adjusted *P*-value for visualization. The data regarding the GO enrichment analysis are shown in [supplementary table S7, Supplementary Material](#) online.

### SH3 Domain Motif Analysis

To identify potential SH3 binding motifs, we used PWMs for each SH3 domain constructed from quantitative motif binding assays (Tonikian et al. 2009; Jain and Bader 2016). We first created a null distribution of MSS by creating a randomized protein set with the same length as the HRR25 orthologs with amino acid frequencies of the *S. cerevisiae* proteome.

For each ortholog-PWM combination, the highest scoring motif was selected to represent the motif score, unless multiple values were observed above the 95th percentile of the random distribution ( $\text{MSS} = 0.64$ ). The full list of MSS values for each ortholog-PWM combination is shown in [supplementary table S8, Supplementary Material](#) online.

### Microscopy Experiments

Cells expressing the mEGFP fusion orthologs were grown until early log phase, by first culturing overnight in 5 mL of SC complete medium + NAT, and diluted to 1:50 in fresh medium 3 h prior to imaging. The cells were then seeded on 0.05 mg/mL concanavalin A-coated (Millipore-Sigma) 96-well glass bottom plate (Cellvis, P96-1.5H-N). Image acquisition was performed using a Nikon Eclipse TE2000-U inverted microscope equipped with a Perkin Elmer UltraVIEW confocal spinning disk unit, a Plan Apochromat DIC H 100×/1.4 oil objective (Nikon), and a Hamamatsu Orca Flash 4.0 LT + camera. Imaging was done at 30 °C in an environmental chamber. The software NIS-Elements (Nikon) was used for image capture. Cells were excited with a 488 nm laser set at 60% intensity and emission was filtered with a 530/630 nm filter to acquire GFP fluorescence. For each field, 1 brightfield and 5 Z-stacked (2  $\mu\text{m}$  apart) fluorescence images were acquired.

### Gene Expression Analysis

Gene expression datasets for *S. cerevisiae*, *K. lactis*, and *N. castellii* were downloaded from the Gene Expression Omnibus with accession IDs GSE36599 (Xue-Franzén et al. 2013), GSE22198 (Tsankov et al. 2010), and GSE90041 (Szachnowski et al. 2019). In order to compare ortholog gene expression levels among different datasets, 1:1:1 orthologs for the three species were identified based on the YGOB annotation (Byrne and Wolfe 2005). Gene expression levels were  $\text{Log}_2$  transformed, and normalized by subtracting the mean expression level of 1:1:1 orthologs. The *N. castellii* gene pairs that were maintained from the WGD were examined for expression imbalance among ohnologs. Gene pair information was extracted based on the YGOB annotation (Byrne and Wolfe 2005), and raw read counts were used as a measure of gene expression levels. We note that the position information does not reflect the loci at which the ohnologs are encoded. Expression imbalance was computed by taking the ratio between the raw read count of ohnolog pairs.

### Essentiality Assay in *N. castellii*

Gene deletion in *N. castellii* was performed as described in Karademir Andersson et al. (2016). First, an antibiotic marker (HPHNT1 or NATNT2) was fused by PCR with 500 bp homology with the promoter and terminator of each ohnolog (NCAS0A01090 and NCAS0D03820). This was achieved by fusion PCR of 3 PCR fragments, each containing the antibiotic marker [amplified from plasmids pFA6a-natNT2 and pFA6a-hphNT1 (Janke et al. 2004)

with homology to 5' and 3' regions of the target gene], the 500 bp 5' region of the target gene, and the 500 bp 3' region of the target gene. Primers used to amplify each fragment are listed in [supplementary table S3, Supplementary Material](#) online.

Genomic integration of the PCR product was performed in the diploid strain obtained by crossing *N. castellii* strains YMC7 and YMC8 (Karademir Andersson et al. 2016). The cells were grown overnight in YPD at room temperature to reach OD<sub>600 nm</sub> around 0.8. The cells were washed once with sterile water and a second time with transformation buffer I (0.1 M lithium acetate, 10 mM Tris-HCl, 1 mM EDTA, pH 7.5). Following the second wash, the pellet was resuspended in 250 µL transformation buffer I. The transformation reaction was set up using 8 µL of the PCR fusion, 2 µL DNA carrier 10 mg/mL with 50 µL competent cells and 300 µL transformation buffer II (40% PEG 3350, 1× transformation buffer I). The reaction was incubated 30 min at room temperature followed by a 30 min heat shock at 30 °C. After the heat shock, the cells were washed twice with 1 mL of sterile water before being resuspended in 100 µL of sterile water for plating on YPD plates with the appropriate antibiotics (HPH 200 µg/mL and NAT 50 µg/mL). After 3 d at room temperature, isolated colonies were tested by colony PCR (Lööke et al. 2011).

Once deletion was confirmed by PCR, the cells were transferred to sporulation media [0.3 % potassium acetate, 0.1 % yeast extract, 0.05% glucose, 0.01% amino acid supplement powder (2 g histidine, 10 g leucine, 2 g lysine, 2 g uracil), 2.0% Agar] for tetrad dissection. After 5 d on sporulation media, cells were resuspended in zymolyase 20T solution (200 µg/mL) for 20 min at room temperature. Following the zymolyase treatment, cells were spun down for 15 s at 16,000 × g and resuspended in 200 µL sorbitol 1 M. Treated cells were then placed on a level YPD plate to perform tetrad dissection with the SporePlay (Singer Instrument). The dissection plates were incubated at room temperature for 5 d to make sure we did not underestimate growth. Once the spores were adequately grown, each spore (by keeping tetrad association) was resuspended in 200 µL sterile water, and 5 µL was spotted on YPD, YPD + NAT (50 µg/mL), YPD + HPH (200 µg/mL), and YPD + G418 (75 µg/mL) for viability evaluation.

## Supplementary Material

[Supplementary material](#) is available at *Molecular Biology and Evolution* online.

## Acknowledgments

The *N. castellii* strain CBS 4309 was a kind gift from Dr Kenneth H. Wolfe. The *N. castellii* strain YMC7 and YMC8 were a kind gift from Dr Marita Cohn. The F65V-34a-mEGFP plasmid was a kind gift from Dr Michael Springer. Molecular graphics was visualized with UCSF ChimeraX, developed by the Resource for Biocomputing,

Visualization, and Informatics at the University of California, San Francisco, with support from National Institutes of Health R01-GM129325 and the Office of Cyber Infrastructure and Computational Biology, National Institute of Allergy and Infectious Diseases. This project was partially funded by a Canadian Institutes of Health Research Foundation grant number 387697 and an NSERC discovery grant to C.R.L. This work was also supported by the JSPS DC1 fellowship (to D.E.-Y.), TTCK fellowship (to D.E.-Y.), Watanabe Foundation International Scholarship (to D.E.-Y.), and MITACS fellowship (to G.S.). C.R.L. holds the Canada Research Chair in Cellular Systems and Synthetic Biology.

## Author Contributions

D.E.-Y. and C.R.L. designed the study. C.R.L. supervised the work. D.E.-Y., G.S., A.K.D., and I.G.-A. prepared the material for assays using *S. cerevisiae*. D.E.-Y., G.S., and A.K.D. performed the complementation and PPI assays. A.K.D. operated the S&P robotic platform for complementation and PPI assays. S.P. performed the imaging experiments. A.K.D. performed the Western blot analysis and experiments using *N. castellii*. D.E.-Y. performed all analyses with support from D.B. and input from C.R.L. D.E.-Y. and C.R.L. wrote the initial draft of the manuscript. D.E.-Y., A.K.D., G.S., S.P., D.B., and C.R.L. contributed to revising, reading, and approving the final version of the manuscript.

## Data Availability

The data from this article are available in the article and in its online [supplementary material](#). Biological resources are available through Addgene (Article #28243453, <https://www.addgene.org/plasmids/articles/28243453/>) or by request to the corresponding author. The computer codes and control files, defining the settings for the codeml program execution, are available at GitHub ([https://github.com/Landrylab/Evans-Yamamoto\\_et\\_al\\_2023](https://github.com/Landrylab/Evans-Yamamoto_et_al_2023), last accessed 2023 November 10).

## References

- Abascal F, Zardoya R, Telford MJ. TranslatorX: multiple alignment of nucleotide sequences guided by amino acid translations. *Nucleic Acids Res.* 2010;**38**(Web Server issue):W7–W13. <https://doi.org/10.1093/nar/gkq291>.
- Altschul SF, Gish W, Miller W, Myers EW, Lipman DJ. Basic local alignment search tool. *J Mol Biol.* 1990;**215**(3):403–410. [https://doi.org/10.1016/S0022-2836\(05\)80360-2](https://doi.org/10.1016/S0022-2836(05)80360-2).
- Álvarez-Carretero S, Kapli P, Yang Z. Beginner's guide on the use of PAML to detect positive selection. *Mol Biol Evol.* 2023;**40**(4):msad041. <https://doi.org/10.1093/molbev/msad041>.
- Anderson BL, Boldogh I, Evangelista M, Boone C, Greene LA, Pon LA. The Src homology domain 3 (SH3) of a yeast type I myosin, Myo5p, binds to verprolin and is required for targeting to sites of actin polarization. *J Cell Biol.* 1998;**141**(6):1357–1370. <https://doi.org/10.1083/jcb.141.6.1357>.
- Ascencio D, Diss G, Gagnon-Arsenault I, Dubé AK, DeLuna A, Landry CR. Expression attenuation as a mechanism of



- robustness against gene duplication. *Proc Natl Acad Sci U S A*. 2021;**118**(6):e2014345118. <https://doi.org/10.1073/pnas.2014345118>.
- Byrne KP, Wolfe KH. The Yeast Gene Order Browser: combining curated homology and syntenic context reveals gene fate in polyploid species. *Genome Res*. 2005;**15**(10):1456–1461. <https://doi.org/10.1101/gr.3672305>.
- Byrne KP, Wolfe KH. Consistent patterns of rate asymmetry and gene loss indicate widespread neofunctionalization of yeast genes after whole-genome duplication. *Genetics*. 2007;**175**(3):1341–1350. <https://doi.org/10.1534/genetics.106.066951>.
- Corbett KD, Harrison SC. Molecular architecture of the yeast monopolin complex. *Cell Rep*. 2012;**1**(6):583–589. <https://doi.org/10.1016/j.celrep.2012.05.012>.
- Cullati SN, Akizuki K, Chen J-S, Gould KL. Substrate displacement of CK1 C-termini regulates kinase specificity. *bioRxiv* 547285. <https://doi.org/10.1101/2023.06.30.547285>, 1 July 2023, preprint: not peer reviewed.
- Deori NM, Nagotu S. Peroxisome biogenesis and inter-organelle communication: an indispensable role for Pex11 and Pex30 family proteins in yeast. *Curr Genet*. 2022;**68**(5–6):537–550. <https://doi.org/10.1007/s00294-022-01254-y>.
- Dionne U, Bourgault É, Dubé AK, Bradley D, Chartier FJM, Dandage R, Dibychintan S, Després PC, Gish GD, Pham NTH, et al. Protein context shapes the specificity of SH3 domain-mediated interactions in vivo. *Nat Commun*. 2021;**12**(1):1597. <https://doi.org/10.1038/s41467-021-21873-2>.
- Diss G, Gagnon-Arsenault I, Dion-Coté A-M, Vignaud H, Ascencio DI, Berger CM, Landry CR. Gene duplication can impart fragility, not robustness, in the yeast protein interaction network. *Science*. 2017;**355**(6325):630–634. <https://doi.org/10.1126/science.aai7685>.
- Donoghue PC, Purnell MA. Genome duplication, extinction and vertebrate evolution. *Trends Ecol Evol*. 2005;**20**(6):312–319. <https://doi.org/10.1016/j.tree.2005.04.008>.
- Evans-Yamamoto D, Rouleau FD, Nanda P, Makanae K, Liu Y, Després PC, Matsuo H, Seki M, Dubé AK, Ascencio D, et al. Barcode fusion genetics-protein-fragment complementation assay (BFG-PCA): tools and resources that expand the potential for binary protein interaction discovery. *Nucleic Acids Res*. 2022;**50**(9):e54. <https://doi.org/10.1093/nar/gkac045>.
- Force A, Lynch M, Pickett FB, Amores A, Yan YL, Postlethwait J. Preservation of duplicate genes by complementary, degenerative mutations. *Genetics*. 1999;**151**(4):1531–1545. <https://doi.org/10.1093/genetics/151.4.1531>.
- Ghaemmaghami S, Huh W-K, Bower K, Howson RW, Belle A, Dephoure N, O'Shea EK, Weissman JS. Global analysis of protein expression in yeast. *Nature*. 2003;**425**(6959):737–741. <https://doi.org/10.1038/nature02046>.
- Ghalei H, Schaub FX, Doherty JR, Noguchi Y, Roush WR, Cleveland JL, Stroupe ME, Karbstein K. Hrr25/CK1δ-directed release of Ltv1 from pre-40S ribosomes is necessary for ribosome assembly and cell growth. *J Cell Biol*. 2015;**208**(6):745–759. <https://doi.org/10.1083/jcb.201409056>.
- Giaever G, Chu AM, Ni L, Connelly C, Riles L, Véronneau S, DowS, Lucau-Danila A, Anderson K, André B, et al. Functional profiling of the *Saccharomyces cerevisiae* genome. *Nature*. 2002;**418**(6896):387–391. <https://doi.org/10.1038/nature00935>.
- Gibson DG. Synthesis of DNA fragments in yeast by one-step assembly of overlapping oligonucleotides. *Nucleic Acids Res*. 2009;**37**(20):6984–6990. <https://doi.org/10.1093/nar/gkp687>.
- Gibson DG, Young L, Chuang R-Y, Venter JC, Hutchison CA III, Smith HO. Enzymatic assembly of DNA molecules up to several hundred kilobases. *Nat Methods*. 2009;**6**(5):343–345. <https://doi.org/10.1038/nmeth.1318>.
- Gout J-F, Lynch M. Maintenance and loss of duplicated genes by dosage subfunctionalization. *Mol Biol Evol*. 2015;**32**(8):2141–2148. <https://doi.org/10.1093/molbev/msv095>.
- Gueldeiner U, Heinisch J, Koehler GJ, Voss D, Hegemann JH. A second set of loxP marker cassettes for Cre-mediated multiple gene knockouts in budding yeast. *Nucleic Acids Res*. 2002;**30**(6):e23. <https://doi.org/10.1093/nar/30.6.e23>.
- Henikoff S, Henikoff JG. Amino acid substitution matrices from protein blocks. *Proc Natl Acad Sci U S A*. 1992;**89**(22):10915–10919. <https://doi.org/10.1073/pnas.89.22.10915>.
- Hishigaki H, Nakai K, Ono T, Tanigami A, Takagi T. Assessment of prediction accuracy of protein function from protein–protein interaction data. *Yeast*. 2001;**18**(6):523–531. <https://doi.org/10.1002/yea.706>.
- Hoekstra MF, Liskay RM, Ou AC, DeMaggio AJ, Burbee DG, Heffron F. HRR25, a putative protein kinase from budding yeast: association with repair of damaged DNA. *Science*. 1991;**253**(5023):1031–1034. <https://doi.org/10.1126/science.1887218>.
- Hughes AL. The evolution of functionally novel proteins after gene duplication. *Proc Biol Sci*. 1994;**256**(1346):119–124. <https://doi.org/10.1098/rspb.1994.0058>.
- Hughes TR, Marton MJ, Jones AR, Roberts CJ, Stoughton R, Armour CD, Bennett HA, Coffey E, Dai H, He YD, et al. Functional discovery via a compendium of expression profiles. *Cell*. 2000;**102**(1):109–126. [https://doi.org/10.1016/S0092-8674\(00\)00015-5](https://doi.org/10.1016/S0092-8674(00)00015-5).
- Innan H, Kondrashov F. The evolution of gene duplications: classifying and distinguishing between models. *Nat Rev Genet*. 2010;**11**(2):97–108. <https://doi.org/10.1038/nrg2689>.
- Jain S, Bader GD. Predicting physiologically relevant SH3 domain mediated protein–protein interactions in yeast. *Bioinformatics*. 2016;**32**(12):1865–1872. <https://doi.org/10.1093/bioinformatics/btw045>.
- Janke C, Magiera MM, Rathfelder N, Taxis C, Reber S, Maekawa H, Moreno-Borchart A, Doenges G, Schwob E, Schiebel E, et al. A versatile toolbox for PCR-based tagging of yeast genes: new fluorescent proteins, more markers and promoter substitution cassettes. *Yeast*. 2004;**21**(11):947–962. <https://doi.org/10.1002/yea.1142>.
- Johri P, Gout J-F, Doak TG, Lynch M. A population-genetic lens into the process of gene loss following whole-genome duplication. *Mol Biol Evol*. 2022;**39**(6):msac118. <https://doi.org/10.1093/molbev/msac118>.
- Kamrad S, Rodríguez-López M, Cotobal C, Correia-Melo C, Ralser M, Bähler J. Pyphe, a python toolbox for assessing microbial growth and cell viability in high-throughput colony screens. *Elife*. 2020;**9**:e55160. <https://doi.org/10.7554/eLife.55160>.
- Karademir Andersson A, Oredsson S, Cohn M. Development of stable haploid strains and molecular genetic tools for *Naumovozyma castellii* (*Saccharomyces castellii*). *Yeast*. 2016;**33**(12):633–646. <https://doi.org/10.1002/yea.3213>.
- Katoh K, Standley DM. MAFFT multiple sequence alignment software version 7: improvements in performance and usability. *Mol Biol Evol*. 2013;**30**(4):772–780. <https://doi.org/10.1093/molbev/mst010>.
- Kondrashov FA. Gene dosage and duplication. In: Dittmar K, Liberles D, editors. *Evolution after gene duplication*. Hoboken (NJ): Wiley; 2010. p. 57–76. <https://doi.org/10.1002/9780470619902.ch4>.
- Kondrashov FA, Rogozin IB, Wolf YI, Koonin EV. Selection in the evolution of gene duplications. *Genome Biol*. 2002;**3**(2):RESEARCH0008. <https://doi.org/10.1186/gb-2002-3-2-research0008>.
- Kozlov AM, Darriba D, Flouri T, Morel B, Stamatakis A. RAxML-NG: a fast, scalable and user-friendly tool for maximum likelihood phylogenetic inference. *Bioinformatics*. 2019;**35**(21):4453–4455. <https://doi.org/10.1093/bioinformatics/btz305>.
- Kung JE, Jura N. Prospects for pharmacological targeting of pseudokinases. *Nat Rev Drug Discov*. 2019;**18**(7):501–526. <https://doi.org/10.1038/s41573-019-0018-3>.
- Laurent JM, Garge RK, Teufel AI, Wilke CO, Kachroo AH, Marcotte EM. Humanization of yeast genes with multiple human orthologs reveals functional divergence between paralogs. *PLoS Biol*. 2020;**18**(5):e3000627. <https://doi.org/10.1371/journal.pbio.3000627>.

- Lee ME, DeLoache WC, Cervantes B, Dueber JE. A highly characterized yeast toolkit for modular, multipart assembly. *ACS Synth Biol.* 2015;**4**(9):975–986. <https://doi.org/10.1021/sb500366v>.
- Li Y, Steenwyk JL, Chang Y, Wang Y, James TY, Stajich JE, Spatafora JW, Groenewald M, Dunn CW, Hittinger CT, et al. A genome-scale phylogeny of the kingdom Fungi. *Curr Biol.* 2021;**31**(8):1653–1665.e5. <https://doi.org/10.1016/j.cub.2021.01.074>.
- Löoke M, Kristjuhan K, Kristjuhan A. Extraction of genomic DNA from yeasts for PCR-based applications. *Biotechniques.* 2011;**50**(5):325–328. <https://doi.org/10.2144/000113672>.
- Louca S, Doebeli M. Efficient comparative phylogenetics on large trees. *Bioinformatics.* 2018;**34**(6):1053–1055. <https://doi.org/10.1093/bioinformatics/btx701>.
- Marchant A, Cisneros AF, Dub AK, Gagnon-Arsenault I, Ascencio D, Jain H, Aub S, Eberlein C, Evans-Yamamoto D, Yachie N, et al. The role of structural pleiotropy and regulatory evolution in the retention of heteromers of paralogs. *eLife.* 2019;**8**:e46754. <https://doi.org/10.7554/eLife.46754>.
- Marcotte EM, Pellegrini M, Thompson MJ, Yeates TO, Eisenberg D. A combined algorithm for genome-wide prediction of protein function. *Nature.* 1999;**402**(6757):83–86. <https://doi.org/10.1038/47048>.
- Mayer ML, Hieter P. Protein networks-built by association. *Nat Biotechnol.* 2000;**18**(12):1242–1243. <https://doi.org/10.1038/82342>.
- Milne DM, Looby P, Meek DW. Catalytic activity of protein kinase CK1 delta (casein kinase 1delta) is essential for its normal subcellular localization. *Exp Cell Res.* 2001;**263**(1):43–54. <https://doi.org/10.1006/excr.2000.5100>.
- Murakami A, Kimura K, Nakano A. The inactive form of a yeast casein kinase I suppresses the secretory defect of the sec12 mutant. Implication of negative regulation by the Hrr25 kinase in the vesicle budding from the endoplasmic reticulum. *J Biol Chem.* 1999;**274**(6):3804–3810. <https://doi.org/10.1074/jbc.274.6.3804>.
- Ohno S. Other mechanisms for achieving gene duplication. In: Ohno S, editor. *Evolution by gene duplication*. Berlin, Heidelberg: Springer; 1970. p. 107–110.
- Otto SP, Whitton J. Polyploid incidence and evolution. *Annu Rev Genet.* 2000;**34**(1):401–437. <https://doi.org/10.1146/annurev.genet.34.1.401>.
- Pajic P, Pavlidis P, Dean K, Neznanova L, Romano R-A, Garneau D, Daugherty E, Globig A, Ruhl S, Gokcumen O. Independent amylase gene copy number bursts correlate with dietary preferences in mammals. *eLife.* 2019;**8**:e44628. <https://doi.org/10.7554/eLife.44628>.
- Peng Y, Grassart A, Lu R, Wong CC, Yates J III, Barnes G, Drubin DG. Casein kinase 1 promotes initiation of clathrin-mediated endocytosis. *Dev Cell.* 2015a;**32**(2):231–240. <https://doi.org/10.1016/j.devcel.2014.11.014>.
- Peng Y, Moritz M, Han X, Giddings TH, Lyon A, Kollman J, Winey M, Yates J III, Agard DA, Drubin DG, et al. Interaction of CK1 $\delta$  with  $\gamma$ TuSc ensures proper microtubule assembly and spindle positioning. *Mol Biol Cell.* 2015b;**26**(13):2505–2518. <https://doi.org/10.1091/mbc.E14-12-1627>.
- Perry GH, Dominy NJ, Claw KG, Lee AS, Fiegler H, Redon R, Werner J, Villanea FA, Mountain JL, Misra R, et al. Diet and the evolution of human amylase gene copy number variation. *Nat Genet.* 2007;**39**(10):1256–1260. <https://doi.org/10.1038/ng2123>.
- Petronczki M, Matos J, Mori S, Gregan J, Bogdanova A, Schwickart M, Mechtler K, Shirahe K, Zachariae W, Nasmyth K. Monopolar attachment of sister kinetochores at meiosis I requires casein kinase 1. *Cell.* 2006;**126**(6):1049–1064. <https://doi.org/10.1016/j.cell.2006.07.029>.
- Pettersen EF, Goddard TD, Huang CC, Meng EC, Couch GS, Croll TI, Morris JH, Ferrin TE. UCSF ChimeraX: structure visualization for researchers, educators, and developers. *Protein Sci.* 2021;**30**(1):70–82. <https://doi.org/10.1002/pro.3943>.
- Pfaffenwimmer T, Reiter W, Brach T, Nogellova V, Papinski D, Schuschnig M, Abert C, Ammerer G, Martens S, Kraft C. Hrr25 kinase promotes selective autophagy by phosphorylating the cargo receptor Atg19. *EMBO Rep.* 2014;**15**(8):862–870. <https://doi.org/10.15252/embr.201438932>.
- Qian W, Liao B-Y, Chang AY-F, Zhang J. Maintenance of duplicate genes and their functional redundancy by reduced expression. *Trends Genet.* 2010;**26**(10):425–430. <https://doi.org/10.1016/j.tig.2010.07.002>.
- Rochette S, Diss G, Filteau M, Leducq J-B, Dubé AK, Landry CR. Genome-wide protein–protein interaction screening by protein-fragment complementation assay (PCA) in living cells. *J Vis Exp.* 2015(97):e52255. <https://doi.org/10.3791/52255>.
- Romero-Calvo I, Ocón B, Martínez-Moya P, Suárez MD, Zarzuelo A, Martínez-Augustín O, de Medina FS. Reversible Ponceau staining as a loading control alternative to actin in Western blots. *Anal Biochem.* 2010;**401**(2):318–320. <https://doi.org/10.1016/j.ab.2010.02.036>.
- Rual J-F, Venkatesan K, Hao T, Hirozane-Kishikawa T, Dricot A, Li N, Berriz GF, Gibbons FD, Dreze M, Ayivi-Guedehoussou N, et al. Towards a proteome-scale map of the human protein–protein interaction network. *Nature.* 2005;**437**(7062):1173–1178. <https://doi.org/10.1038/nature04209>.
- Scannell DR, Frank AC, Conant GC, Byrne KP, Woolfit M, Wolfe KH. Independent sorting-out of thousands of duplicated gene pairs in two yeast species descended from a whole-genome duplication. *Proc Natl Acad Sci U S A.* 2007;**104**(20):8397–8402. <https://doi.org/10.1073/pnas.0608218104>.
- Scannell DR, Wolfe KH. A burst of protein sequence evolution and a prolonged period of asymmetric evolution follow gene duplication in yeast. *Genome Res.* 2008;**18**(1):137–147. <https://doi.org/10.1101/gr.6341207>.
- Shen X-X, Opulente DA, Kominek J, Zhou X, Steenwyk JL, Buh KV, Haase MAB, Wisecaver JH, Wang M, Doering DT, et al. Tempo and mode of genome evolution in the budding yeast subphylum. *Cell.* 2018;**175**(6):1533–1545.e20. <https://doi.org/10.1016/j.cell.2018.10.023>.
- Szachnowski U, Andjus S, Foretek D, Morillon A, Wery M. Endogenous RNAi pathway evolutionarily shapes the destiny of the antisense lncRNAs transcriptome. *Life Sci Alliance.* 2019;**2**(5):e201900407. <https://doi.org/10.26508/lsa.201900407>.
- Tanaka K, Matsui Y. Functions of unconventional myosins in the yeast *Saccharomyces cerevisiae*. *Cell Struct Funct.* 2001;**26**(6):671–675. <https://doi.org/10.1247/csf.26.671>.
- Tanaka C, Tan L-J, Mochida K, Kirisako H, Koizumi M, Asai E, Sakoh-Nakatogawa M, Ohsumi Y, Nakatogawa H. Hrr25 triggers selective autophagy-related pathways by phosphorylating receptor proteins. *J Cell Biol.* 2014;**207**(1):91–105. <https://doi.org/10.1083/jcb.201402128>.
- Tarassov K, Messier V, Landry CR, Radinovic S, Serna Molina MM, Shames I, Malitskaya Y, Vogel J, Bussey H, Michnick SW. An in vivo map of the yeast protein interactome. *Science.* 2008;**320**(5882):1465–1470. <https://doi.org/10.1126/science.1153878>.
- Tonikian R, Xin X, Toret CP, Gfeller D, Landgraf C, Panni S, Paoluzi S, Castagnoli L, Currell B, Seshagiri S, et al. Bayesian modeling of the yeast SH3 domain interactome predicts spatiotemporal dynamics of endocytosis proteins. *PLoS Biol.* 2009;**7**(10):e1000218. <https://doi.org/10.1371/journal.pbio.1000218>.
- Tsankov AM, Thompson DA, Socha A, Regev A, Rando OJ. The role of nucleosome positioning in the evolution of gene regulation. *PLoS Biol.* 2010;**8**(7):e1000414. <https://doi.org/10.1371/journal.pbio.1000414>.
- van Hoof A. Conserved functions of yeast genes support the duplication, degeneration and complementation model for gene duplication. *Genetics.* 2005;**171**(4):1455–1461. <https://doi.org/10.1534/genetics.105.044057>.
- Wang J, Davis S, Menon S, Zhang J, Ding J, Cervantes S, Miller E, Jiang Y, Ferro-Novick S. Ypt1/Rab1 regulates Hrr25/CK1 $\delta$  kinase activity in ER-Golgi traffic and macroautophagy. *J Cell Biol.* 2015;**210**(2):273–285. <https://doi.org/10.1083/jcb.201408075>.
- Wang L-G, Lam TT-Y, Xu S, Dai Z, Zhou L, Feng T, Guo P, Dunn CW, Jones BR, Bradley T, et al. Treeio: an R package for phylogenetic

- tree input and output with richly annotated and associated data. *Mol Biol Evol.* 2020;**37**(2):599–603. <https://doi.org/10.1093/molbev/msz240>.
- Wolfe KH, Armisen D, Proux-Wera E, ÓhÉigeartaigh SS, Azam H, Gordon JL, Byrne KP. Clade- and species-specific features of genome evolution in the Saccharomycetaceae. *FEMS Yeast Res.* 2015;**15**(5):fov035. <https://doi.org/10.1093/femsyr/fov035>.
- Xue-Franzén Y, Henriksson J, Bürglin TR, Wright APH. Distinct roles of the Gcn5 histone acetyltransferase revealed during transient stress-induced reprogramming of the genome. *BMC Genomics.* 2013;**14**(1):479. <https://doi.org/10.1186/1471-2164-14-479>.
- Yang Z. PAML 4: phylogenetic analysis by maximum likelihood. *Mol Biol Evol.* 2007;**24**(8):1586–1591. <https://doi.org/10.1093/molbev/msm088>.
- Ye Q, Ur SN, Su TY, Corbett KD. Structure of the *Saccharomyces cerevisiae* Hrr25:Mam1 monopolin subcomplex reveals a novel kinase regulator. *EMBO J.* 2016;**35**(19):2139–2151. <https://doi.org/10.15252/embj.201694082>.
- Yu G, Wang L-G, Han Y, He Q-Y. clusterProfiler: an R package for comparing biological themes among gene clusters. *OMICS.* 2012;**16**(5):284–287. <https://doi.org/10.1089/omi.2011.0118>.
- Zhang B, Butler AM, Shi Q, Xing S, Herman PK. P-body localization of the Hrr25/casein kinase 1 protein kinase is required for the completion of meiosis. *Mol Cell Biol.* 2018;**38**(17):e00678–e00678. <https://doi.org/10.1128/MCB.00678-17>.
- Zhang B, Shi Q, Varia SN, Xing S, Klett BM, Cook LA, Herman PK. The activity-dependent regulation of protein kinase stability by the localization to P-bodies. *Genetics.* 2016;**203**(3):1191–1202. <https://doi.org/10.1534/genetics.116.187419>.